

Unitary Coupled-Cluster based Self-Consistent Electron Propagator Theory for Electron-Detached and Electron-Attached States: A Quadratic Unitary Coupled-Cluster Singles and Doubles Method and Benchmark Calculations

Yu Zhang and Junzi Liu*

*School of Chemistry and Biological Engineering, University of Science and Technology
Beijing, Beijing 100083, China*

E-mail: jliu413@ustb.edu.cn

Abstract

A unitary coupled-cluster (UCC)-based self-consistent electron propagator theory (EPT) is proposed for the description of electron-detached and electron-attached states. Two practical schemes, termed IP/EA-UCC3 and IP/EA-qUCCSD, are developed and implemented within the UCC singles and doubles (UCCSD) framework using the perturbative and commutator-based truncation strategies for the similarity-transformed Hamiltonian \bar{H} . The numerical performance of these UCC-based EPT methods is evaluated primarily using full configuration interaction (FCI) reference data and compared with established approaches, including IP/EA-ADC(3), IP/EA-ADC(4) and IP/EA-

EOM-CCSD. Benchmark calculations demonstrate that IP-qUCCSD achieves the highest overall accuracy among Hermitian ionized-state methods for one-hole (1h)-dominated IPs of closed-shell systems, with a mean absolute deviation (MAD) of 0.19 eV and standard deviation (SD) of 0.13 eV. Remarkably, despite the absence of triple-excitation contributions, IP-qUCCSD outperforms the higher-order ADC(4) method. For one-particle (1p)-dominated EA calculations, all tested methods exhibit comparable accuracy.

1 Introduction

Propagator theory provides a general and powerful framework in quantum chemistry for describing the dynamical and response properties of many-electron systems through the formalism of propagators, also known as many-body Green’s functions.^{1–16} It comprises two principal branches: the polarization propagator theory (PPT) and electron propagator theory (EPT). PPT characterizes neutral excitations by modeling how perturbations in the electron density propagate through a correlated many-electron system, thereby yielding excitation energies (EEs) and related properties. In contrast, EPT focuses on single-particle propagation, providing direct access to electron binding energies, including ionization potentials (IPs) and electron affinities (EAs). Together, PPT and EPT constitute a unified theoretical formalism for describing both charged and neutral excitations in molecules and condensed phase. The present work focuses on EPT, while detailed developments of PPT are presented in refs. 5,17–48. Owing to its rigorous treatment of electron correlation and its direct connection to optical and X-ray photoelectron spectra,^{49,50} EPT-based approaches have become powerful and extensively developed tools for electronic-structure and spectroscopic studies.

The electron propagator $G(\omega)$ (one-particle Green’s function) is formally related to the non-interacting Green’s function $G^0(\omega)$ through the Dyson equation, in which electron correlation beyond the mean-field approximation and orbital relaxation effects are incorporated via the nonlocal, frequency-dependent effective one-particle potential $\Sigma(\omega)$, commonly re-

ferred to as the self-energy.¹⁶ In practice, solving the Dyson equation requires suitable approximations to $\Sigma(\omega)$, which are typically constructed using diagrammatic perturbation theory. This leads to a variety of finite-order perturbative expansion approaches, including the outer valence Green’s function (OVGF) method,^{3,4} the diagonal second order (D2) method,^{51–53} the diagonal third order (D3) method,⁵³ Dyson equation-based algebraic diagrammatic construction (Dyson-ADC) methods,^{9,54–56} the two-particle-one-hole Tamm-Dancoff approximation (2p1h-TDA),⁵⁷ the partial third-order (P3) method,⁵⁸ the quasiparticle third-order (Q3) method,⁵⁹ and the linear third-order (L3) methods,⁵⁹ along with their various renormalized extensions and variants.^{59–62} Collectively, these can be called Dyson-type approaches. Within Dyson-type EPT, the electron-attachment and electron-detachment processes are treated simultaneously through a coupled description of the $(N \pm 1)$ -electron states. On the other hand, the electron propagator can be rigorously decomposed into a spectral representation by introducing a complete set of $(N \pm 1)$ -electron states and the exact ground-state wavefunction. This decomposition naturally gives rise to forward and backward components of electron propagator, corresponding to electron attachment and detachment, respectively. Within this formulation, the approximated ground-state and the $(N \pm 1)$ -electron states can be employed explicitly, thereby avoiding the need to solve the Dyson equation; such methods are therefore often referred to as non-Dyson (nD) approaches. In this context, several non-Dyson approaches have been formulated and implemented, including the nD-D2, nD-D3, nD-L3,^{62,63} and nD-ADC methods.^{64–69} In contrast to Dyson-type methods, non-Dyson approaches decouple electron attachment and electron-detachment components of the electron propagator, making them conceptually more transparent and computationally more efficient. It is notable that the ADC family of methods is perhaps the most popular EPT/PPT approach, attracting considerable interest as a Hermitian excited-state framework that offers a favorable balance between computational efficiency and accuracy. Over the past decades, ADC methods for computing electron-detached and electron-attached energies, as well as the related properties, have been systematically developed to various perturbative orders

through diagrammatic techniques,^{64,66,70} the intermediate state representation (ISR) framework,^{30,65,71–77} and effective Liouvillean theory.^{67,78}

Among the various approaches related to EPT, those based on coupled-cluster theory – such as the coupled-cluster Green’s function (CCGF) method,^{79–85} the symmetry-adapted cluster configuration interaction (SAC-CI) method,^{86–90} and the equation-of-motion coupled-cluster (EOM-CC)^{91–101} /linear-response CC (LR-CC) theories^{102–109} – have established themselves as state-of-the-art tools for the accurate and reliable description of $(N \pm 1)$ -electron states.^{110–113} In particular, the IP/EA-EOM-CC approaches provide a hierarchy of size-intensive methods whose accuracy can be systematically improved by including contributions from higher excitations, ranging from singles and doubles to triples and even quadruples.^{114–123} In addition, several simplified EOM-CC-based variants for computing IPs and EAs have been developed.^{124–131} However, because the similarity-transformed Hamiltonians in EOM-CC/LR-CC methods are non-Hermitian, they may yield complex excitation energies,¹³² especially near conical intersections between electronic states of the same symmetry.^{133–138} This limitation has motivated the development of Hermitian formulation within the CC framework.^{42,43,139–149}

Besides the methods discussed above, the self-consistent operator expansion offers another valuable route for solving the equations of the polarization/electron propagator theories.^{6,150–152} Nearly forty years ago, Mukherjee and co-workers proposed a compact formulation of self-consistent propagator theory that employs a unitary couple-cluster (UCC) ground-state wavefunction together with a self-consistent excitation manifold constructed from unitary-transformed excitation operator.¹⁵¹ This formulation uses the UCC ansatz to generate N -representable ground and excited states, enabling a Hermitian and non-perturbative treatment of neutral and charged excitations through the decoupling of forward and backward propagator components. More recently, the working equations of UCC-based self-consistent polarization propagator theory have been derived and implemented on efficient computational platforms.^{42–44} Because the similarity-transformed Hamiltonian \bar{H} in

UCC is non-terminating, two practical truncation schemes have been developed: a third-order perturbative approach (UCC3)⁴² and a quadratic commutator-truncated approach (qUCCSD).⁴³ These methods have been extensively benchmarked and consistently exhibit systematic performance improvements from UCC3 to qUCCSD.^{44,45} Notably, the strict third-order UCC-PPT method (UCC3-s) has been shown to be formally equivalent to the strict third-order ADC method (ADC(3)-s, commonly referred to ADC(3)).⁴² Subsequently, the theoretical connection between UCC-based PPT and the intermediate state representation (ISR) formulation of ADC methods has been established.^{32,46,153} Building on this connection, UCC3 schemes for computing IPs and EAs have been implemented and compared with their ADC counterparts.^{154–156} Nevertheless, a rigorous and explicit derivation of the working equations for UCC-based EPT using the self-consistent operator expansion is still lacking. Moreover, qUCCSD approaches for IP and EA calculations have not yet been implemented and systematically benchmarked. It therefore remains an open question whether the systematic improvements observed from UCC3 to qUCCSD within polarization propagator theory will extend in a similar manner to the electron propagator framework.

In this work, we rigorously derive UCC-EPT using the self-consistent operator expansion and present implementations of both the third-order (IP/EA-UCC3) and quadratic commutator-truncated (IP/EA-qUCCSD) approaches. By integrating UCC theory with the self-consistent propagator framework, these methods provide a Hermitian, non-perturbative and systematically improvable alternative to conventional IP/EA-EOM-CC approaches. Their performance is evaluated through extensive benchmarks and compared with established ADC methods and IP/EA-EOM-CCSD, enabling a direct assessment of accuracy, robustness, and computational cost. This paper is organized as follows: section 2 presents the theoretical derivation of working equations and introduces the third-order and quadratic UCCSD schemes for computing IPs and EAs; section 3 summarize the computational details; section 4 discusses benchmark results and comparisons among IP/EA-EOM-CCSD, IP/EA-ADC(3), IP/EA-ADC(4), IP/EA-UCC3, and IP/EA-qUCCSD methods; and concluding remarks and

outlooks are given in section 5.

2 Theory

2.1 Electron propagator theory

A matrix element of the electron propagator $G_{p,r}(\omega)$ in the frequency domain is defined as

$$G_{p,r}(\omega) = \langle \Psi_{\text{gr}}^N | [\hat{a}_p, (\omega \hat{I} + \hat{H})^{-1} \hat{a}_r^\dagger]_- | \Psi_{\text{gr}}^N \rangle, \quad (1)$$

where Ψ_{gr}^N denotes the exact ground-state wavefunction of the N -electron system, and \hat{a}_r^\dagger and \hat{a}_p are the fermionic creation and annihilation operators, respectively. The notation $[]_-$ represents the anticommutator, $[A, B]_- = AB + BA$, and is used here because the expression contains an odd number of fermionic operators (either \hat{a}_p or \hat{a}_r^\dagger). The action of the superoperator \hat{H} of the Hamiltonian \hat{H} on an arbitrary operator \hat{A} gives the commutator of \hat{A} and \hat{H} , namely, $\hat{H}\hat{A} = [\hat{A}, \hat{H}]$; while the identity superoperator \hat{I} satisfies $\hat{I}\hat{A} = \hat{A}$. The spectral representation of the one-particle propagator can be decomposed into forward $G_{p,r}^+(\omega)$ and backward $G_{p,r}^-(\omega)$ components:

$$G_{p,r}(\omega) = G_{p,r}^+(\omega) + G_{p,r}^-(\omega) \quad (2)$$

$$G_{p,r}^+(\omega) = \sum_L \frac{\langle \Psi_{\text{gr}}^N | \hat{a}_p | \Psi_L^{N+1} \rangle \langle \Psi_L^{N+1} | \hat{a}_r^\dagger | \Psi_{\text{gr}}^N \rangle}{\omega - (E_L^{N+1} - E_{\text{gr}}^N)} \quad (3)$$

$$G_{p,r}^-(\omega) = \sum_K \frac{\langle \Psi_{\text{gr}}^N | \hat{a}_r^\dagger | \Psi_K^{N-1} \rangle \langle \Psi_K^{N-1} | \hat{a}_p | \Psi_{\text{gr}}^N \rangle}{\omega + (E_K^{N-1} - E_{\text{gr}}^N)} \quad (4)$$

where $G_{p,r}^+(\omega)$ and $G_{p,r}^-(\omega)$ correspond to electron-attachment and electron-detachment processes, respectively. The sets $\{\Psi_L^{N+1}\}$ and $\{\Psi_K^{N-1}\}$ denote complete bases of $(N+1)$ and $(N-1)$ -electron states with associated energies E_L^{N+1} and E_K^{N-1} . The exact ground-state and excited-state wavefunctions are not accessible in practical implementations of electron propagator theory. Therefore, approximate ground-state wavefunctions and incomplete manifold

of excited states are employed. To decouple the forward and backward components of the propagator, the approximate wavefunction must satisfy the so-called “vacuum annihilation condition” (VAC).^{6,150,151} Self-consistent propagator theories^{6,150–152,157} enforce this decoupling by constructing self-consistent excitation operators that satisfy the VAC. The unitary coupled-cluster (UCC) ansatz can be directly integrated into this self-consistent propagator framework. In recent years, UCC-based self-consistent polarization propagator theory has been formulated, derived, and implemented.^{42–44} The generality of this formalism enables its extension to a corresponding self-consistent electron propagator theory, providing a foundation for UCC-based Hermitian approaches to $(N \pm 1)$ -electron states.

2.2 UCC-based self-consistent electron propagator theory

The basic theoretical framework of UCC has been presented in our previous work.^{42,43} For a self-contained presentation, we briefly recapitulate its key contents here. In UCC theory, the ground-state wavefunction $|\Psi_{\text{gr}}\rangle$ is written as a unitary exponential operator acting on a reference state $|\Phi_0\rangle$, typically the Hartree-Fock determinant:

$$|\Psi_{\text{gr}}\rangle = e^{\hat{\sigma}}|\Phi_0\rangle. \quad (5)$$

Unlike the conventional coupled-cluster theory, the cluster operator $\hat{\sigma}$ in UCC is defined as $\hat{\sigma} = \hat{T} - \hat{T}^\dagger$ and is therefore anti-Hermitian, $\hat{\sigma}^\dagger = -\hat{\sigma}$. Consequently, the wave operator $e^{\hat{\sigma}}$ is unitary:

$$(e^{\hat{\sigma}})^\dagger = e^{-\hat{\sigma}} = (e^{\hat{\sigma}})^{-1}. \quad (6)$$

In the UCC singles and doubles (UCCSD) model, the excitation and de-excitation operators are

$$\hat{T} = \sum_{ai} \sigma_i^a \{\hat{a}_a^\dagger \hat{a}_i\} + \frac{1}{4} \sum_{abij} \sigma_{ij}^{ab} \{\hat{a}_a^\dagger \hat{a}_b^\dagger \hat{a}_j \hat{a}_i\}, \quad (7)$$

$$\hat{T}^\dagger = \sum_{ai} (\sigma_i^a)^* \{\hat{a}_i^\dagger \hat{a}_a\} + \frac{1}{4} \sum_{abij} (\sigma_{ij}^{ab})^* \{\hat{a}_i^\dagger \hat{a}_j^\dagger \hat{a}_b \hat{a}_a\}, \quad (8)$$

where $\{i, j, \dots\}$, $\{a, b, \dots\}$ and $\{p, q, \dots\}$ denote occupied, virtual, and arbitrary orbitals, respectively, and σ_i^a and σ_{ij}^{ab} are the ground-state cluster amplitudes. The UCCSD ground-state energy and amplitude equations are

$$E_{\text{gr}} = \langle \Phi_0 | \bar{H} | \Phi_0 \rangle, \quad (9)$$

$$0 = \langle \Phi_l | \bar{H} | \Phi_0 \rangle, \quad (10)$$

where $\{\Phi_l\}$ comprises the singly and doubly excited determinants, i.e., $\{\Phi_i^a\}$ and $\{\Phi_{ij}^{ab}\}$. Here $\bar{H} = e^{-\hat{\sigma}} \hat{H} e^{\hat{\sigma}}$ is the Hermitian similarity-transformed Hamiltonian. The projected amplitude equations not only determine the ground-state amplitudes but also ensure the block-diagonal structure of the matrix representation of the electron propagator, as discussed below.

In UCC-based self-consistent electron propagator theory, the self-consistent operator manifolds for electron detachment and electron attachment are $\{\hat{z}_I^\dagger\} \cup \{\hat{z}_I\}$ and $\{\hat{z}_A^\dagger\} \cup \{\hat{z}_A\}$, respectively. Both manifolds are formed from unitary-transformed excitation and de-excitation operators,

$$\hat{z}_I^\dagger = e^{\hat{\sigma}} \hat{b}_I^\dagger e^{-\hat{\sigma}}, \quad \hat{z}_A^\dagger = e^{\hat{\sigma}} \hat{b}_A^\dagger e^{-\hat{\sigma}}, \quad (11)$$

where \hat{b}_I^\dagger and \hat{b}_A^\dagger denote the original electron-detachment and electron-attachment operators, respectively. In the UCCSD model, we adopt the form $\{\hat{b}_I^\dagger\} = \{\hat{a}_i\} \cup \{\hat{a}_a^\dagger \hat{a}_j \hat{a}_i\}$ for electron detachment and $\{\hat{b}_A^\dagger\} = \{\hat{a}_a^\dagger\} \cup \{\hat{a}_a^\dagger \hat{a}_b^\dagger \hat{a}_i\}$ for electron attachment. To streamline the derivation,

we introduce the binary product notation

$$(X|Y) = \langle \Psi_{\text{gr}}^N | [X, Y^\dagger]_- | \Psi_{\text{gr}}^N \rangle, \quad (12)$$

so that the electron propagator can be rewritten as

$$G_{p,r}(\omega) = \langle \Psi_{\text{gr}}^N | [\hat{a}_p, (\omega \hat{I} + \hat{H})^{-1} \hat{a}_r^\dagger]_- | \Psi_{\text{gr}}^N \rangle = (\hat{a}_p | (\omega \hat{I} - \hat{H})^{-1} \hat{a}_r). \quad (13)$$

We introduce the superoperator resolution of identity within the subspaces spanned by the self-consistent operators (including both electron-attachment and electron-detachment operators):¹⁵¹

$$\hat{I} = \sum_A |\hat{z}_A\rangle \langle \hat{z}_A| + \sum_I |\hat{z}_I^\dagger\rangle \langle \hat{z}_I^\dagger|, \quad (14)$$

$$(X|Y) = \sum_A (X|\hat{z}_A) \langle \hat{z}_A|Y) + \sum_I (X|\hat{z}_I^\dagger) \langle \hat{z}_I^\dagger|Y). \quad (15)$$

By inserting the resolution of identity [eq. (14)-(15)] into the binary product form of $G_{p,r}(\omega)$ [eq. (13)], a matrix form of the electron propagator is obtained,

$$G(\omega)_{p,r} = M_p D^{-1}(\omega) M_r^\dagger, \quad (16)$$

where M_p and M_r^\dagger contain both electron-attachment and electron-detachment components,

$$M_p = \begin{pmatrix} (M_+)_{p,A} & (M_-)_{p,I} \end{pmatrix} = \begin{pmatrix} (\hat{a}_p | \hat{z}_A) & (\hat{a}_p | \hat{z}_I^\dagger) \end{pmatrix}, \quad (17)$$

$$M_r^\dagger = \begin{pmatrix} (M_+)_{B,r} \\ (M_-)_{J,r} \end{pmatrix} = \begin{pmatrix} (\hat{z}_B | \hat{a}_r) \\ (\hat{z}_J^\dagger | \hat{a}_r) \end{pmatrix}. \quad (18)$$

The matrix D has a 2×2 block structure,

$$D = \begin{pmatrix} D_{++} & D_{+-} \\ D_{-+} & D_{--} \end{pmatrix}, \quad (19)$$

with matrix elements

$$(D_{++})_{AB} = (\hat{z}_A | (\omega \hat{I} - \hat{H}) | \hat{z}_B), \quad (20)$$

$$(D_{--})_{IJ} = (\hat{z}_I^\dagger | (\omega \hat{I} - \hat{H}) | \hat{z}_J^\dagger), \quad (21)$$

$$(D_{+-})_{AJ} = (\hat{z}_A | (\omega \hat{I} - \hat{H}) | \hat{z}_J^\dagger), \quad (22)$$

$$(D_{-+})_{IB} = (\hat{z}_I^\dagger | (\omega \hat{I} - \hat{H}) | \hat{z}_B). \quad (23)$$

Consistent with VAC, the off-diagonal blocks simplify to

$$(D_{+-})_{AJ} = \langle \Phi_0 | \hat{b}_A \hat{b}_J \bar{H} | \Phi_0 \rangle = 0, \quad (24)$$

$$(D_{-+})_{IB} = -\langle \Phi_0 | \bar{H} \hat{b}_B^\dagger \hat{b}_I^\dagger | \Phi_0 \rangle = 0. \quad (25)$$

A product of electron-attachment and electron-detachment operators ($\hat{b}_A \hat{b}_J$ and $\hat{b}_B^\dagger \hat{b}_I^\dagger$) constitutes a conventional excitation operator; hence $\hat{b}_B^\dagger \hat{b}_I^\dagger | \Phi_0 \rangle$ and $\langle \Phi_0 | \hat{b}_A \hat{b}_J$ correspond to excited determinants and their Hermitian conjugates. Therefore, eq. (24)-(25) are precisely the projected UCC amplitude equations. It follows that D is block-diagonal and the forward and backward components of electron propagator decouple:

$$D = \begin{pmatrix} D_{++} & 0 \\ 0 & D_{--} \end{pmatrix}. \quad (26)$$

The diagonal blocks D_{++} and D_{--} comprise matrix elements of \bar{H} :

$$(D_{++})_{AB} = \delta_{AB}\omega - (\bar{H})_{AB}, \quad (\bar{H})_{AB} = \langle \Phi_0 | \hat{b}_A \bar{H} \hat{b}_B^\dagger | \Phi_0 \rangle, \quad (27)$$

$$(D_{--})_{IJ} = \delta_{IJ}\omega - (\bar{H})_{IJ}, \quad (\bar{H})_{IJ} = \langle \Phi_0 | \hat{b}_I \bar{H} \hat{b}_J^\dagger | \Phi_0 \rangle. \quad (28)$$

The energies of electron-detached and electron-attached states are obtained from the poles of the corresponding electron propagator components, leading to eigenvalue equations for the transformed Hamiltonian \bar{H} within the spaces spanned by $\{b_I^\dagger\}$ and $\{b_A^\dagger\}$:

$$\sum_J (\bar{H})_{IJ} C_{JK} = E_K C_{IK}, \quad \sum_B (\bar{H})_{AB} C_{BL} = E_L C_{AL}. \quad (29)$$

The corresponding wavefunctions are

$$\Psi_K^{\text{IP}} = \sum_I C_{IK} e^{\hat{\sigma}} \hat{b}_I^\dagger | \Phi_0 \rangle, \quad \Psi_L^{\text{EA}} = \sum_A C_{AL} e^{\hat{\sigma}} \hat{b}_A^\dagger | \Phi_0 \rangle. \quad (30)$$

These eigenvalue equations can also be derived within the intermediate-state representations by employing $\hat{z}_I^\dagger | \Psi_{\text{gr}} \rangle = e^{\hat{\sigma}} \hat{b}_I^\dagger | \Phi_0 \rangle$ and $\hat{z}_A^\dagger | \Psi_{\text{gr}} \rangle = e^{\hat{\sigma}} \hat{b}_A^\dagger | \Phi_0 \rangle$ as the basis for representing the Hamiltonian.³² Within this framework, several related methods have been developed, including IP/EA-ADC(3) and IP/EA-UCC3.^{74,76,155,156}

It is important to emphasize that when a complete set of self-consistent operator manifolds is employed, the decoupling between the forward and backward components of electron propagator is exact. The truncation of the excitation manifolds introduces approximations. For example, the UCCSD amplitude equations guarantee the vanishing of single and double excitations/de-excitations in \bar{H} , yielding exact decoupling between single excitation in the forward propagator and single de-excitations in the backward propagator. By contrast, the decoupling between single excitations in $G_{p,r}^+$ and double de-excitations in $G_{p,r}^-$, as well as between double excitations in $G_{p,r}^+$ and single/double de-excitations in $G_{p,r}^-$, remains approximate because the triple and quadruple excitation/de-excitation terms in \bar{H} do not vanish.

Consequently, the eigenvalue equations [eq. (29)] neglect these residual couplings. Nevertheless, since the one-particle electron propagator theory is primarily used for describing $(N \pm 1)$ -electron states with dominant single-particle or single-hole character, the exact decoupling of single excitations and single de-excitations within the UCCSD-based electron propagator framework is particularly attractive and useful feature.

Within UCCSD model, the components of \bar{H} relevant to the ground-state energy E_{gr} , the amplitude equations (\bar{H}_{ai} and $\bar{H}_{ab,ij}$), and the IP/EA eigenvalue equations can be summarized as

$$\begin{aligned} \bar{H} = & E_{\text{gr}} + \left(\left(\bar{H}_{ai} \{ \hat{a}_a^\dagger \hat{a}_i \} + \frac{1}{4} \bar{H}_{ab,ij} \{ \hat{a}_a^\dagger \hat{a}_b^\dagger \hat{a}_j \hat{a}_i \} \right) + h.c. \right) + \left(\bar{H}_{ij} \{ \hat{a}_i^\dagger \hat{a}_j \} + \bar{H}_{ab} \{ \hat{a}_a^\dagger \hat{a}_b \} + \right. \\ & \left. \frac{1}{4} \bar{H}_{ij,kl} \{ \hat{a}_i^\dagger \hat{a}_j^\dagger \hat{a}_l \hat{a}_k \} + \frac{1}{4} \bar{H}_{ab,cd} \{ \hat{a}_a^\dagger \hat{a}_b^\dagger \hat{a}_d \hat{a}_c \} + \bar{H}_{ia,bj} \{ \hat{a}_i^\dagger \hat{a}_a^\dagger \hat{a}_j \hat{a}_b \} \right) + \left(\left(\frac{1}{2} \bar{H}_{ij,ka} \{ \hat{a}_i^\dagger \hat{a}_j^\dagger \hat{a}_a \hat{a}_k \} \right. \right. \\ & \left. \left. + \frac{1}{2} \bar{H}_{ab,ci} \{ \hat{a}_a^\dagger \hat{a}_b^\dagger \hat{a}_i \hat{a}_c \} \right) + h.c. \right). \end{aligned} \quad (31)$$

The eigenvalue equations for electron-detached (ionized) states can be written in block form as

$$\begin{bmatrix} \bar{H}_{1\text{h}-1\text{h}} & \bar{H}_{1\text{h}-2\text{h}1\text{p}} \\ \bar{H}_{2\text{h}1\text{p}-1\text{h}} & \bar{H}_{2\text{h}1\text{p}-2\text{h}1\text{p}} \end{bmatrix} \begin{bmatrix} C_{1\text{h}} \\ C_{2\text{h}1\text{p}} \end{bmatrix} = E^{\text{IP}} \begin{bmatrix} C_{1\text{h}} \\ C_{2\text{h}1\text{p}} \end{bmatrix}. \quad (32)$$

Here, $\bar{H}_{1\text{h}-1\text{h}}$ is the ‘‘one-hole – one-hole’’ block involving \bar{H}_{ij} ; $\bar{H}_{1\text{h}-2\text{h}1\text{p}}$ and $\bar{H}_{2\text{h}1\text{p}-1\text{h}}$ are the ‘‘one-hole – two-hole-one-particle’’ and ‘‘two-hole-one-particle – one-hole’’ blocks involving $\bar{H}_{ij,ka}$ and $\bar{H}_{ka,ij}$, respectively; and $\bar{H}_{2\text{h}1\text{p}-2\text{h}1\text{p}}$ is the ‘‘two-hole-one-particle – two-hole-one-particle’’ block involving \bar{H}_{ij} , \bar{H}_{ab} , $\bar{H}_{ij,kl}$, and $\bar{H}_{ia,bj}$. Similarly, the eigenvalue equation for electron-attached states takes the block form

$$\begin{bmatrix} \bar{H}_{1\text{p}-1\text{p}} & \bar{H}_{1\text{p}-1\text{h}2\text{p}} \\ \bar{H}_{1\text{h}2\text{p}-1\text{p}} & \bar{H}_{1\text{h}2\text{p}-1\text{h}2\text{p}} \end{bmatrix} \begin{bmatrix} C_{1\text{p}} \\ C_{1\text{h}2\text{p}} \end{bmatrix} = E^{\text{EA}} \begin{bmatrix} C_{1\text{p}} \\ C_{1\text{h}2\text{p}} \end{bmatrix}. \quad (33)$$

Here, $\bar{H}_{1\text{p}-1\text{p}}$ refers to the ‘‘one-particle – one-particle’’ block involving \bar{H}_{ab} ; $\bar{H}_{1\text{p}-1\text{h}2\text{p}}$ and

$\bar{H}_{1\text{h}2\text{p}-1\text{p}}$ are the “one-particle - one-hole-two-particle” and “one-hole-two-particle - one-particle” blocks involving $\bar{H}_{ci,ab}$ and $\bar{H}_{ab,ci}$, respectively; and $\bar{H}_{1\text{h}2\text{p}-1\text{h}2\text{p}}$ is the “one-hole-two-particle - one-hole-two-particle” block involving \bar{H}_{ij} , \bar{H}_{ab} , $\bar{H}_{ab,cd}$, and $\bar{H}_{ia,bj}$.

In contrast to CC theory, where \bar{H} is non-Hermitian and its commutator expansion terminates at quartic power, the \bar{H} in UCC theory is Hermitian and features a non-terminating commutator expansion. We adopt a commutator expansion for \bar{H} with Bernoulli-number prefactors,

$$\bar{H} = \bar{H}^0 + \bar{H}^1 + \bar{H}^2 + \bar{H}^3 + \dots, \quad (34)$$

$$\bar{H}^0 = \hat{F} + \hat{V}, \quad (35)$$

$$\bar{H}^1 = [\hat{F}, \hat{\sigma}] + \frac{1}{2}[\hat{V}, \hat{\sigma}] + \frac{1}{2}[V_R, \sigma], \quad (36)$$

$$\bar{H}^2 = \frac{1}{12}[[\hat{V}_N, \hat{\sigma}], \hat{\sigma}] + \frac{1}{4}[[\hat{V}, \hat{\sigma}]_R, \hat{\sigma}] + \frac{1}{4}[[\hat{V}_R, \hat{\sigma}]_R, \hat{\sigma}] \quad (37)$$

$$\begin{aligned} \bar{H}^3 = & \frac{1}{24}[[[\hat{V}_N, \hat{\sigma}], \hat{\sigma}]_R, \hat{\sigma}] + \frac{1}{8}[[[\hat{V}_R, \hat{\sigma}]_R, \hat{\sigma}]_R, \hat{\sigma}] + \frac{1}{8}[[[\hat{V}, \hat{\sigma}]_R, \hat{\sigma}]_R, \hat{\sigma}] - \frac{1}{24}[[[\hat{V}, \hat{\sigma}]_R, \hat{\sigma}], \hat{\sigma}] - \\ & \frac{1}{24}[[[\hat{V}_R, \hat{\sigma}]_R, \hat{\sigma}], \hat{\sigma}], \end{aligned} \quad (38)$$

where “ N ” denotes the part of an operator consisting of excitation and de-excitation components of the target operator, while “ R ” refers to the reminder that excludes the “ N ” part. The Hamiltonian operator \hat{H} is decomposed into the Fock operator \hat{F} and the fluctuation operator \hat{V} , written in normal-ordered second-quantized form as

$$\hat{F} = \sum_{ij} f_{ij} \{\hat{a}_i^\dagger \hat{a}_j\} + \sum_{ab} f_{ab} \{a_a^\dagger a_b\}, \quad \hat{V} = \frac{1}{4} \sum_{pqrs} \langle pq || rs \rangle \{\hat{a}_p^\dagger \hat{a}_q^\dagger \hat{a}_s \hat{a}_r\}. \quad (39)$$

This Bernoulli expansion avoids all commutators of order higher than the single commutator with respect to \hat{F} and provides a compact form suitable for practical UCCSD implementations. By applying Löwdin partitioning¹⁵⁸ to eq. (32) and (33), the terms associated with the 2h1p (or 1h2p) excitations can be folded into the 1h-1h (or 1p-1p) block. This yields to

the following energy-dependent eigenvalue equation for the 1h-1h (or 1p-1p) block:

$$\left[\bar{H}_{1h-1h} + \bar{H}_{1h-2h1p} (E^{\text{IP}} - \bar{H}_{2h1p-2h1p})^{-1} \bar{H}_{2h1p-1h} \right] C_{1h-1h} = E^{\text{IP}} C_{1h-1h}, \quad (40)$$

$$\left[\bar{H}_{1p-1p} + \bar{H}_{1p-1h2p} (E^{\text{EA}} - \bar{H}_{1h2p-1h2p})^{-1} \bar{H}_{1h2p-1p} \right] C_{1p-1p} = E^{\text{EA}} C_{1p-1p}. \quad (41)$$

In these equations, \bar{H}_{1h-1h} (or \bar{H}_{1p-1p}) primarily governs states dominated by the single-hole (or single-particle) character. The term $\bar{H}_{1h-2h1p}(E^{\text{IP}} - \bar{H}_{2h1p-2h1p})^{-1}\bar{H}_{2h1p-1h}$ (or $\bar{H}_{1p-1h2p}(E^{\text{EA}} - \bar{H}_{1h2p-1h2p})^{-1}\bar{H}_{1h2p-1p}$) can be viewed as corrections to the leading block. A balanced truncation scheme for practical UCC-EPT requires a consistent level of approximation for both the dominant and correction terms. Specifically, the expansion terms retained in \bar{H}_{1h-1h} (or \bar{H}_{1p-1p}) should be one order higher than those in $\bar{H}_{1h-2h1p}/\bar{H}_{2h1p-1h}$ (or $\bar{H}_{1p-1h2p}/\bar{H}_{1h2p-1p}$), and two orders higher than those in $\bar{H}_{2h1p-2h1p}$ (or $\bar{H}_{1h2p-1h2p}$). To achieve third order accuracy within Møller Plesset (MP) perturbation theory for single-hole (or single-particle)-dominated states, the terms in \bar{H}_{1h-1h} (or \bar{H}_{1p-1p}) should be evaluated through third order, the terms in $\bar{H}_{1h-2h1p}/\bar{H}_{2h1p-1h}$ (or $\bar{H}_{1p-1h2p}/\bar{H}_{1h2p-1p}$) through second order, and $\bar{H}_{2h1p-2h1p}$ (or $\bar{H}_{1h2p-1h2p}$) through first order. In addition, the two UCCSD amplitude equations, $\bar{H}_{ai} = 0$ and $\bar{H}_{ab,ij} = 0$, used to iteratively optimize the ground-state amplitudes, can also be evaluated through third order. By analogy with UCC3 in UCC-PPT,⁴² this formulation is termed the IP/EA-UCC3 scheme. For further simplification, substituting the MP3 ground-state amplitudes directly into IP/EA-UCC3 yields a perturbative variant – the strict version of IP/EA-UCC3 (IP/EA-UCC3-s), which is equivalent to the IP/EA-ADC(3) method.^{155,156} An alternative and natural truncation strategy for UCC-based methods is truncation by commutator order. One of the simplest such models in UCC-PPT is the quadratic UCCSD (qUCCSD) scheme.⁴³ Following this strategy, the IP/EA-qUCCSD scheme is readily formulated for calculating IPs and EAs. In IP/EA-qUCCSD, both the ground-state amplitude equations and \bar{H}_{1h-1h} (or \bar{H}_{1p-1p}) block in the electron-detached (or -attached) state eigenvalue equations are truncated to include double commutators between

\hat{V} and $\hat{\sigma}$ in the Bernoulli expansion. Simultaneously, $\bar{H}_{1h-2h1p}$ and $\bar{H}_{2h1p-1h}$ (or $\bar{H}_{1p-1h2p}$ and $\bar{H}_{1h2p-1p}$) are truncated to the single-commutator level, while $\bar{H}_{2h1p-2h1p}$ (or $\bar{H}_{1h2p-1h2p}$) is truncated to the bare Hamiltonian. Compared with IP/EA-UCC3 scheme, the IP/EA-qUCCSD approach includes additional higher-order contributions arising from the commutator structure in both the amplitude equations and electron-detached (or attached)-state eigenvalue equations. In principle, this leads to a systematic improvement over the IP/EA-UCC3 method.

2.3 The working equations for the IP/EA-qUCCSD scheme

The working equations for the IP/EA-qUCCSD method are derived using the Bernoulli expansion of \bar{H} (as outlined in the previous subsection), together with diagrammatic techniques analogous to those employed in UCC-PPT. The expressions for the ground-state energy and the two amplitude equations are identical to those in qUCCSD.⁴³ For completeness, the relevant formulas are collected in the Appendix. Here we focus on the contributions to \bar{H} that enter the various blocks of the electron-detachment and electron-attachment [$(N \pm 1)$ -electron state] eigenvalue equations.

In the IP-qUCCSD approach, the “1h-1h” block of the electron-detachment eigenvalue equation arises solely from \bar{H}_{ij} , truncated at the double-commutator level. The resulting

expressions for $\bar{H}_{ij}^{\text{IP-qUCCSD}}$ can be decomposed as

$$\bar{H}_{ij}^{\text{IP-qUCCSD}} = \bar{H}_{ij}^0 + \bar{H}_{ij}^1 + \bar{H}_{ij}^2, \quad (42)$$

$$\bar{H}_{ij}^0 = f_{ij}, \quad (43)$$

$$\bar{H}_{ij}^1 = \sum_{kab} \frac{1}{4} \langle ik||ab \rangle \sigma_{jk}^{ab} + \sum_{ka} \langle ik||ja \rangle \sigma_k^a + h.c., \quad (44)$$

$$\begin{aligned} \bar{H}_{ij}^2 = & \left(\sum_{klabc} \frac{1}{2} (\sigma_{kl}^{bc})^* \langle ic||al \rangle \sigma_{jk}^{ab} + \sum_{klmab} \frac{1}{8} (\sigma_{kl}^{ab})^* \langle im||kl \rangle \sigma_{jm}^{ab} + h.c. \right) \\ & - \sum_{klmab} \frac{1}{2} (\sigma_{kl}^{ab})^* \langle im||jl \rangle \sigma_{km}^{ab} + \sum_{klabc} \frac{1}{2} (\sigma_{kl}^{ac})^* \langle ic||jb \rangle \sigma_{kl}^{ab} \\ & + \left(\sum_{kabc} \frac{1}{4} (\sigma_k^b)^* \langle ib||ac \rangle \sigma_{jk}^{ac} - \sum_{klab} \frac{1}{2} (\sigma_k^b)^* \langle il||ak \rangle \sigma_{jl}^{ab} + \sum_{klab} \frac{1}{2} (\sigma_l^b)^* \langle ik||ja \rangle \sigma_{kl}^{ab} + h.c. \right) \\ & + \left(\sum_{kab} \frac{5}{12} \langle ik||ab \rangle \sigma_j^a \sigma_k^b + \sum_{kab} \frac{1}{2} (\sigma_k^b)^* \langle ib||ak \rangle \sigma_j^a + h.c. \right) \\ & - \sum_{kla} (\sigma_l^a)^* \langle ik||jl \rangle \sigma_k^a + \sum_{kab} (\sigma_k^a)^* \langle ia||jb \rangle \sigma_k^b. \end{aligned} \quad (45)$$

The $\bar{H}_{1h-2h1p}$ block contains only $\bar{H}_{ij,ka}^{\text{IP-qUCCSD}}$, expanded to the single-commutator level:

$$\bar{H}_{ij,ka}^{\text{IP-qUCCSD}} = \bar{H}_{ij,ka}^0 + \bar{H}_{ij,ka}^1, \quad (46)$$

$$\bar{H}_{ij,ka}^0 = \langle ij||ka \rangle, \quad (47)$$

$$\begin{aligned} \bar{H}_{ij,ka}^1 = & P(ij) \sum_{lb} (\sigma_{jl}^{ab})^* \langle ib||kl \rangle + \sum_{bc} \frac{1}{2} (\sigma_{ij}^{cb})^* \langle bc||ak \rangle + \sum_b \frac{1}{2} \langle ij||ba \rangle \sigma_k^b \\ & - \sum_l (\sigma_l^a)^* \langle ij||kl \rangle - P(ij) \sum_b (\sigma_j^b)^* \langle ib||ak \rangle. \end{aligned} \quad (48)$$

The $\bar{H}_{2h1p-1h}$ block contains $\bar{H}_{ka,ij}$, the Hermitian conjugate of $\bar{H}_{ij,ka}$, i.e., $\bar{H}_{ij,ka} = (\bar{H}_{ka,ij})^*$.

In addition to \bar{H}_{ij}^0 discussed above, the $\bar{H}_{2h1p-2h1p}$ block also contains the bare Hamiltonian

terms corresponding to \bar{H}_{ab}^0 , $\bar{H}_{ia,bj}^0$, and $\bar{H}_{ij,kl}^0$, which are given by

$$\bar{H}_{ab}^{\text{IP-qUCCSD}[0]} = \bar{H}_{ab}^0 = f_{ab}, \quad (49)$$

$$\bar{H}_{ia,bj}^{\text{IP-qUCCSD}} = \bar{H}_{ia,bj}^0 = \langle ia||bj \rangle, \quad (50)$$

$$\bar{H}_{ij,kl}^{\text{IP-qUCCSD}} = \bar{H}_{ij,kl}^0 = \langle ij||kl \rangle. \quad (51)$$

Similarly, in the EA-qUCCSD scheme, the “1p-1p” block of the electron-attachment eigenvalue equation contains only contributions from \bar{H}_{ab} , truncated at the double-commutator level. The corresponding expressions are

$$\bar{H}_{ab}^{\text{EA-qUCCSD}} = \bar{H}_{ab}^0 + \bar{H}_{ab}^1 + \bar{H}_{ab}^2, \quad (52)$$

$$\bar{H}_{ab}^0 = f_{ab}, \quad (53)$$

$$\bar{H}_{ab}^1 = -\sum_{ijc} \frac{1}{4} \langle ij||bc \rangle \sigma_{ij}^{ac} + \sum_{ic} \langle ai||bc \rangle \sigma_i^c + h.c., \quad (54)$$

$$\begin{aligned} \bar{H}_{ab}^2 = & \left(-\sum_{ijkcd} \frac{1}{2} (\sigma_{ij}^{cd})^* \langle kd||bj \rangle \sigma_{ik}^{ca} - \sum_{ijcdf} \frac{1}{8} (\sigma_{ij}^{fd})^* \langle df||cb \rangle \sigma_{ij}^{ac} + h.c. \right) \\ & + \sum_{ijcdf} \frac{1}{2} (\sigma_{ij}^{fd})^* \langle ad||bc \rangle \sigma_{ij}^{fc} - \frac{1}{2} \sum_{ijkcd} (\sigma_{ij}^{cd})^* \langle ka||jb \rangle \sigma_{ik}^{cd} \\ & + \left(\sum_{ijkc} \frac{1}{4} (\sigma_j^c)^* \langle ik||bj \rangle \sigma_{ik}^{ac} - \sum_{ijcd} \frac{1}{2} (\sigma_j^c)^* \langle ic||bd \rangle \sigma_{ij}^{ad} + \sum_{ijcd} \frac{1}{2} (\sigma_j^d)^* \langle ia||cb \rangle \sigma_{ij}^{cd} + h.c. \right) \\ & + \left(-\frac{5}{12} \sum_{ijc} \langle ij||bc \rangle \sigma_i^a \sigma_j^c - \sum_{ijc} \frac{1}{2} (\sigma_j^c)^* \langle ic||bj \rangle \sigma_i^a + h.c. \right) \\ & - \sum_{ijc} (\sigma_i^c)^* \langle ja||ib \rangle \sigma_j^c + \sum_{icd} (\sigma_i^d)^* \langle ad||bc \rangle \sigma_i^c. \end{aligned} \quad (55)$$

The $\bar{H}_{1p-1h2p}$ block includes only $\bar{H}_{ci,ab}^{\text{EA-qUCCSD}}$, expanded up to the single-commutator level.

It is the Hermitian conjugate of $\bar{H}_{ab,ci}^{\text{EA-qUCCSD}}$, which contributes to the $\bar{H}_{1\text{h}2\text{p}-1\text{p}}$ block:

$$\bar{H}_{ab,ci}^{\text{EA-qUCCSD}} = \bar{H}_{ab,ci}^0 + \bar{H}_{ab,ci}^1, \quad (56)$$

$$\bar{H}_{ab,ci}^0 = \langle ab||ci\rangle, \quad (57)$$

$$\begin{aligned} \bar{H}_{ab,ci}^1 &= P(ab) \sum_{jd} \langle aj||cd\rangle \sigma_{ij}^{bd} + \sum_{kj} \frac{1}{2} \langle jk||ci\rangle \sigma_{jk}^{ab} - \sum_j \frac{1}{2} (\sigma_j^c)^* \langle ab||ji\rangle \\ &+ \sum_d \langle ab||cd\rangle \sigma_i^d - P(ab) \sum_j \langle aj||ci\rangle \sigma_j^b. \end{aligned} \quad (58)$$

The $\bar{H}_{1\text{h}2\text{p}-1\text{h}2\text{p}}$ consists of the bare Hamiltonian contributions \bar{H}_{ab}^0 , \bar{H}_{ij}^0 , $\bar{H}_{ab,cd}^0$, and $\bar{H}_{ia,bj}^0$.

In fact, \bar{H}_{ab}^0 , \bar{H}_{ij}^0 , and $\bar{H}_{ia,bj}^0$ in $\bar{H}_{1\text{h}2\text{p}-1\text{h}2\text{p}}$ block are identical to those in $\bar{H}_{2\text{h}1\text{p}-2\text{h}1\text{p}}$ block:

$$\bar{H}_{ab}^{\text{IP-qUCCSD}} = \bar{H}_{ab}^{\text{EA-qUCCSD}[0]} = f_{ab}, \quad \bar{H}_{ij}^{\text{IP-qUCCSD}[0]} = \bar{H}_{ij}^{\text{EA-qUCCSD}}, \quad \bar{H}_{ia,bj}^{\text{IP-qUCCSD}} = \bar{H}_{ia,bj}^{\text{EA-qUCCSD}}. \quad (59)$$

The $\bar{H}_{ab,cd}^{\text{EA-qUCCSD}}$ contributes exclusively to $\bar{H}_{2\text{h}1\text{p}-2\text{h}1\text{p}}$ and equals the bare Hamiltonian,

$$\bar{H}_{ab,cd}^{\text{EA-qUCCSD}} = \bar{H}_{ab,cd}^0 = \langle ab||cd\rangle. \quad (60)$$

It is worth noting that the amplitude equations and target-state eigenvalue equations in the IP/EA-UCC3 scheme constitute a subset of those in IP/EA-qUCCSD. Thus, IP/EA-UCC3 can be straightforwardly obtained by omitting terms beyond third order in the qUCCSD ground-state amplitude equations and in the $\bar{H}_{1\text{h}-1\text{h}}^{\text{IP-qUCCSD}} / \bar{H}_{1\text{p}-1\text{p}}^{\text{EA-qUCCSD}}$ block; terms beyond second order in the $\bar{H}_{1\text{h}-2\text{h}1\text{p}}^{\text{IP-qUCCSD}} (\bar{H}_{2\text{h}1\text{p}-1\text{h}}^{\text{IP-qUCCSD}}) / \bar{H}_{1\text{p}-1\text{h}2\text{p}}^{\text{EA-qUCCSD}} (\bar{H}_{1\text{h}2\text{p}-1\text{p}}^{\text{EA-qUCCSD}})$ blocks; and terms beyond first order in the $\bar{H}_{2\text{h}1\text{p}-2\text{h}1\text{p}}^{\text{IP-qUCCSD}} / \bar{H}_{1\text{h}2\text{p}-1\text{h}2\text{p}}^{\text{EA-qUCCSD}}$ block. The connection between IP/EA-UCC3 and IP/EA-ADC(3) has been discussed in refs. 155 and 156. Figure 1 illustrates the block structure and constituents of \bar{H} in the electron-attachment and electron-detachment eigenvalue equations discussed above. For comparison, the corresponding IP/EA-UCC3 block structure and components are also shown.

2.4 Relation between working equations of UCC-EPT and UCC-PPT

At the level of working equations, UCC-based EPT and PPT share the same ground-state amplitude equations for a given truncation scheme. Moreover, the structure of the $(N \pm 1)$ -electron state eigenvalue equations in UCC-EPT closely parallels that of the excited-state eigenvalue equations in UCC-PPT. Within the UCCSD model, both frameworks yield 2×2 block-type eigenvalue equations. In the qUCCSD scheme,⁴³ the \bar{H}_{SS} block provides the largest contribution to excitation energies dominated by single-excitation character; likewise, the \bar{H}_{1h-1h} and \bar{H}_{1p-1p} blocks contribute most to the IPs of 1h-dominated electron-detached states and to the EAs of 1p-dominated electron-attached state, respectively. Hence, each corresponding block in the 2×2 block matrices serves a comparable role within the eigenvalue equations of the two frameworks. The key distinction between UCC-EPT and UCC-PPT lies in the specific terms included in the respective blocks: each block in the $(N \pm 1)$ -electron state eigenvalue equations of UCC-EPT contains a subset of the terms present in the corresponding excited-state eigenvalue equations of UCC-PPT. The relevant \bar{H} components of the qUCCSD and IP/EA-qUCCSD eigenvalue equations are summarized in Table 1. In the IP-qUCCSD scheme, the \bar{H}_{1h-1h} , $\bar{H}_{1h-2h1p}$, and $\bar{H}_{2h1p-1h}$ blocks draw their contributions solely from \bar{H}_{ij} , $\bar{H}_{ij,ka}$, and $\bar{H}_{ci,ab}$, respectively – terms that also constitute parts of \bar{H}_{SS} , \bar{H}_{SD} and \bar{H}_{DS} in qUCCSD. The \bar{H}_{DD} block in qUCCSD includes an additional $\bar{H}_{ab,cd}$ contribution that is absent from the $\bar{H}_{2h1p-2h1p}$ block of IP-qUCCSD. Analogous relationships hold for the EA-qUCCSD method. Consequently, once UCC-PPT equations are derived and implemented, the corresponding UCC-EPT formulations can be constructed directly and efficiently, since all required \bar{H} terms are already available within the UCC-PPT framework.

The overall formal scalings of the ground-state amplitude equations and the $(N \pm 1)$ -electron state eigenvalue equations in the IP/EA-qUCCSD method are $\mathcal{O}(N^6)$ and $\mathcal{O}(N^5)$, respectively – identical to those of IP/EA-EOM-CCSD. Because the ground-state theory of IP/EA-qUCCSD is the same as that of qUCCSD, the computational cost of solving the

ground-state amplitude equations is approximately twice that of a CCSD calculation.⁴⁴ Compared with IP/EA-ADC(3) (also referred to as IP/EA-UCC3-s), both IP/EA-qUCCSD and IP/EA-UCC3 are substantially more demanding, as they require iterative optimizations of the ground-state amplitudes rather than using perturbative amplitudes. The solutions of the eigenvalue equations for IP- and EA-qUCCSD scale as $\mathcal{O}(N_o^3 N_v^2)$ and $\mathcal{O}(N_o N_v^4)$, respectively, matching the formal scaling of IP/EA-EOM-CCSD. In practice, IP/EA-qUCCSD is slightly less computationally expensive than IP/EA-EOM-CCSD. In IP/EA-EOM-CCSD, the similarity-transformed Hamiltonian \bar{H} contains three-body terms – namely, $\frac{1}{2} \sum_{mnef} t_{ij}^{ae} \langle mn || ef \rangle r_{mn}^f$ in the $\bar{H}_{2h1p-2h1p}$ block and $-\frac{1}{2} \sum_{klcd} t_{kj}^{ab} \langle kl || cd \rangle r_l^{cd}$ in the $\bar{H}_{1h2p-1h2p}$ block – both arising from $[\hat{V}, \hat{T}_2]$ in the BCH expansion. By contrast, in IP/EA-qUCCSD the $\bar{H}_{2h1p-2h1p}$ and $\bar{H}_{1h2p-1h2p}$ blocks are constructed directly from the bare Hamiltonian in the Bernoulli expansion of the $\bar{H}^{\text{IP/EA-qUCCSD}}$; thus, no three-body terms appear in its eigenvalue equations. Moreover, coupling terms such as $\sum_{me} \bar{H}_{me} r_{mi}^e$ in $\bar{H}_{1h-2h1p}$ block and $\sum_{me} \bar{H}_{me} r_m^{ae}$ in $\bar{H}_{1p-1h2p}$ block – present in IP/EA-EOM-CCSD – do not contribute in the UCC-based PPT/EPT formulation as well. This follows from the Hermiticity of \bar{H}^{UCC} together with the amplitude equations, which enforce the vanishing of the $\bar{H}_{me}^{\text{qUCCSD}}$. Consequently, IP/EA-qUCCSD avoids these contributions, leading to a lower overall computational cost compared to IP/EA-EOM-CCSD. The construction of the similarity-transformed Hamiltonian \bar{H} in the IP/EA-qUCCSD also scales as $\mathcal{O}(N^6)$, as in qUCCSD. In contrast, UCC-EPT calculations are generally less computationally intensive than qUCCSD, since fewer \bar{H} terms appear in the various blocks of the eigenvalue equations – particularly in the cost-dominating blocks \bar{H}_{1h-1h} for IP-qUCCSD and \bar{H}_{1p-1p} for EA-qUCCSD. On the other hand, IP/EA-qUCCSD remains somewhat more expensive than IP/EA-EOM-CCSD because additional $\mathcal{O}(N_o^4 N_v^2)$ and $\mathcal{O}(N_o^3 N_v^3)$ terms are required when constructing \bar{H} , especially in these cost-dominating blocks. Nevertheless, these $\mathcal{O}(N^6)$ -scaling intermediates are computed only once and can be reused in subsequent solutions of the eigenvalue equations.

3 Computational details

The IP/EA-UCC3 and IP/EA-qUCCSD methods were implemented in the PySCF software package¹⁵⁹ using generalized orbital formulation. Building on existing UCC3 and qUCCSD implementations, the programs for IP/EA-UCC3 and IP/EA-qUCCSD described in section 2 were reorganized and extended. The correctness of the UCC3 and qUCCSD implementations in PySCF was verified by comparison with our earlier implementation in the X2CSOCC module¹⁶⁰ of the CFOUR program.^{161,162} Benchmark calculations of one-hole (1h)-dominated vertical IPs (VIPs) were performed using the dataset from ref. 75 and compared with IP-EOM-CCSD, IP-ADC(3), IP-ADC(4), and IP-UCC3. This benchmark set comprises 25 VIPs from closed-shell systems (six neutral molecules and four anions) and 17 VIPs from open-shell systems (two radicals, three neutral triplet molecules, and four radical anions), providing a broad and representative assessment. Reference VIPs were obtained from full configuration interaction (FCI) calculations, with the exception of CO, HCN, NO_2^- , NO_2^\bullet and $\text{HCN}^{\bullet-}$, which were calculated using configuration interaction with singles, doubles, triples, and quadruples (CISDTQ). In addition, a dataset¹⁶³ of 201 1h-dominated VIPs was used for further benchmarking. In this dataset, high-level reference values were computed using the IP-EOM-CCSDT method. The set spans 42 molecules with closed-shell singlet ground states, offering a robust statistical basis for error analysis. Benchmark calculations of vertical EAs (VEAs) dominated by one-particle (1p)-dominated VEAs were conducted using the dataset from ref. 76 and compared with EA-EOM-CCSD, EA-ADC(3), EA-ADC(4), and EA-UCC3. This VEA benchmark dataset includes 35 VEAs from 10 closed-shell systems (seven neutral molecules and three cations) containing up to three second-row atoms, as well as 16 VEAs from 8 open-shell systems (two radicals, three neutral triplet molecules, and three radical cations). Reference VEAs were obtained using FCI or, for CO, HCN, NO_2^+ and NO_2^\bullet , CISDTQ. To enable comparison with existing ADC benchmarks, all datasets were selected to match the statistical scopes reported in prior studies.⁷⁵⁻⁷⁷ In all calculations, standard non-relativistic two-electron integrals were used without approximation, and the

1s orbitals of non-hydrogen atoms were kept frozen. Detailed geometries of all test systems and the basis sets employed are provided in the Supporting Information (SI). They can also be found in the original references.^{75,76,163}

4 Results and discussion

4.1 Benchmark calculations of ionization potentials (IPs)

A statistical analysis of the deviations in 25 IPs for closed-shell reference states, calculated by IP-qUCCSD, IP-UCC3, IP-ADC(3), IP-ADC(4), and IP-EOM-CCSD relative to FCI reference data, is presented in Table 2. The corresponding vertical IPs computed with these methods are listed in Table S1 of the Supporting Information. For Hermitian excited-state methods, the two UCC-based approaches generally outperform the ADC counterparts for 1h-dominated electron-detached states. This trend contrasts with that observed for excitation energies (EEs), where qUCCSD performs nearly identically to ADC(3).^{44,45} Specifically, IP-UCC3 yields a mean absolute deviation ($\text{MAD} = \frac{1}{n} \sum_i^n |\Delta_i|$, $\Delta_i = E_i^{\text{calc}} - E_i^{\text{FCI}}$) comparable to IP-ADC(4) but with a lower standard deviation ($\text{SD} = \sqrt{\frac{1}{n} \sum_i^n (\Delta_i - \bar{\Delta})^2}$), whereas IP-qUCCSD further improves upon IP-ADC(4), reducing the MAD and SD by 30% and 52%, respectively. In principle, IP-ADC(3), IP-UCC3 and IP-qUCCSD can all be regarded as “third-order methods”, capable of achieving IPs accurate to the third order. In IP-qUCCSD, iterative optimization of ground-state amplitudes, together with fourth- and fifth-order contributions entering via the double commutator in the electron-detachment eigenvalue equation, yields a noticeably improved description of 1h-dominated VIPs compared to IP-ADC(3). From a theoretical perspective, one would therefore expect IP-ADC(4) – a formal fourth-order method – to surpass both IP-UCC3 and IP-qUCCSD in accuracy. However, IP-qUCCSD clearly outperforms IP-ADC(4) despite omitting triple-excitation contributions and the fourth-order terms arising from the triple commutators. A comparison of the mean deviation ($\text{MD} = \frac{1}{n} \sum_i^n \Delta_i$, $\Delta_i = E_i^{\text{calc}} - E_i^{\text{FCI}}$), maximum positive devia-

tion ($\text{MaxD}(+) = \max(\{\Delta_i\})$), and minimum negative deviation ($\text{MinD}(-) = \min(\{\Delta_i\})$) between IP-ADC(3) and IP-ADC(4), along with their median deviations and overall distributions depicted in the violin plots (Figure 2), shows that IP-ADC(3) tends to overestimate VIPs, whereas IP-ADC(4) tends to underestimate them. When IP-ADC(2) and other IP-ADC(4) variants are also considered,⁷⁷ an oscillatory convergence pattern emerges within the ADC family, with ADC(4) apparently overcorrecting the deficiencies of ADC(3). This behavior suggests that simple inclusion of higher-order terms in the MP perturbation expansion for the amplitudes does not necessarily yield a systematic improvement in accuracy for the ADC family of methods. Instead of a fixed-order MP expansion of the amplitudes, the commutator-truncation scheme in qUCCSD treats the cluster amplitudes consistently and is more compatible with the self-consistent solution of the amplitude equations. Collectively, these considerations may explain the unexpectedly superior performance relative to IP-ADC(4).

Similar to the UCC3 versus qUCCSD case,^{43,45} IP-qUCCSD consistently improves upon IP-UCC3, reducing the MAD and SD by 0.06 eV and 0.05 eV, respectively. Among the four Hermitian methods evaluated, IP-qUCCSD delivers the best overall numerical performance. This conclusion is further supported by benchmark calculations of 201 VIPs with closed-shell reference states from the CGB dataset reported in Ref 163. The complete list of VIPs computed using the examined methods is provided in Table S4 of the Supporting Information. As shown in Table 3, the deviation statistics increase for all methods on the CGB dataset. The expanded dataset and the use of IP-EOM-CCSDT reference values significantly affect the deviation distributions, particularly by amplifying both $\text{MaxD}(+)$ and $\text{MinD}(-)$ across methods. Despite the resulting increases in MAD and SD for the UCC-based approaches, IP-UCC3 performs comparably to IP-ADC(4), while IP-qUCCSD maintains a clear advantage, with MAD and SD values lower than those of IP-ADC(4) by 0.04 eV and 0.05 eV, respectively. Overall, IP-qUCCSD remains the most accurate of the four Hermitian methods examined. On the 25-VIP dataset, IP-EOM-CCSD attains slightly higher accuracy than IP-qUCCSD,

with a lower MAD of 0.11 eV and the same SD of 0.13 eV. When applied to the CGB dataset, both IP-EOM-CCSD and IP-qUCCSD show increased deviations, with a more pronounced deterioration for IP-EOM-CCSD (its MAD and SD more than double relative to the 25-VIP set). In this case, IP-qUCCSD matches the MAD of IP-EOM-CCSD but achieves a lower SD of 0.22 eV and exhibits less severe negative outlier. Within the exception of IP-ADC(4), all methods tend to overestimate the vertical IPs. The MD, MaxD(+) and MinD(-) values for IP-UCC3 and IP-qUCCSD reveal a decreasing degree of overestimation, further underscoring the systematic improvement from IP-UCC3 to IP-qUCCSD. Taken together, these statistical results indicate that the performance of IP-qUCCSD approaches that of IP-EOM-CCSD. This finding highlights the potential for further development of more accurate methods within the UCC-EPT framework, both to explore the limitations of the current UCCSD model and to clarify the correspondence between the UCCSD truncation scheme and IP-EOM-CCSD accuracy.

By utilizing different reference states, IP/EA methods can target $(N \pm 1)$ -electron states that differ by a single electron from the reference. It is therefore essential to assess the performance of UCC-EPT for systems with open-shell references. Table 4 summarizes the statistical deviations for 17 1h-character VIPs with open-shell reference from ref. 75, computed by IP-qUCCSD, IP-UCC3, IP-ADC(3), IP-ADC(4), and IP-EOM-CCSD relative to FCI. The full list of calculated VIPs is provided in Table S3 of the Supporting Information. Among the five methods, IP-ADC(4) delivers the highest accuracy and precision, reflecting the important role of triple excitations in computing VIPs for open-shell reference systems. For IP-qUCCSD, the MAD and SD exceed those of IP-ADC(4) both by about 0.03 eV, and its MaxD(+) is substantially larger. Nevertheless, a slight improvement over IP-UCC3 persists for open-shell systems. Overall, IP-qUCCSD performs nearly on par with IP-EOM-CCSD and clearly surpasses IP-ADC(3).

4.2 Benchmark calculations of electron affinities (EAs)

A statistical analysis of deviations in 35 VEAs with closed-shell reference states and 16 VEAs with open-shell reference states, calculated using EA-qUCCSD, EA-UCC3, EA-ADC(3), EA-ADC(4), and EA-EOM-CCSD relative to FCI reference data, is presented in Table 5 and Table 6, respectively. The complete sets of VEAs computed by these methods are documented in Table S6 and S7 of the Supporting Information. For 1p-dominated VEAs with closed-shell references, the methods show no significant difference: all yield MADs of approximately 0.05 eV and SDs around 0.10 eV. Across methods, the VEA deviations fall within roughly -0.20 eV to +0.50 eV. Unlike the VIP case, no clear improvement is observed when moving from ADC(3) to ADC(4) or from UCC3 to qUCCSD; three CC-based methods display a slight tendency to underestimate VEAs on average, as reflected in their median deviations and vertical position of violin plots (Figure 3). Over the 10 closed-shell molecules examined, the Hermitian methods perform comparably to EA-EOM-CCSD, producing accurate and reliable electron-attachment energies. For 1p-character VEAs with open-shell references, EA-ADC(4) demonstrates the highest accuracy and precision among all methods, with a MAD of 0.03 eV and an SD of 0.06 eV – as expected for a higher-order approach relative to the other Hermitian methods. Although the MAD and SD of EA-EOM-CCSD are higher than those of EA-ADC(4) by 0.05 eV and 0.06 eV, respectively, it still outperforms the other three Hermitian methods. The performance of EA-qUCCSD closely matches that of EA-ADC(3), consistent with trends reported for excitation-energy benchmarks of qUCCSD and ADC(3). By contrast, EA-UCC3 is slightly worse than EA-ADC(3), suggesting that higher-order contributions beyond third order in the double commutators – arising from the ground-state amplitude equations and the electron-attachment eigenvalue equations – tend to overcorrect the VEAs.

5 Conclusion and outlook

In this work, we derived the working equations of unitary coupled-cluster (UCC) based electron propagator theory using self-consistent operator manifolds. Two practical schemes within the UCCSD model were implemented for computing vertical ionization potentials (VIPs) and electron affinities (VEAs): a perturbation-truncated approach (IP/EA-UCC3) and a commutator-truncated approach (IP/EA-qUCCSD). Benchmark calculations across five datasets were used to assess the accuracy and precision of IP/EA-UCC3 and IP/EA-qUCCSD for 1h-dominated VIPs and 1p-dominated VEAs. For systems with closed-shell reference states, IP-qUCCSD achieved the highest accuracy among the Hermitian methods considered, outperforming both formally third-order approaches – IP-UCC3 and IP-ADC(3) – and even the higher-order IP-ADC(4). For open-shell systems, IP-qUCCSD performed comparably to IP-ADC(4); in both closed- and open-shell systems, a consistent improvement from UCC3 to qUCCSD was observed. For VEAs with closed-shell references, all tested methods exhibit nearly identical performance. For the open-shell systems, EA-qUCCSD attained accuracy similar to EA-ADC(3), reflecting trends seen for excitation energy calculations, whereas EA-ADC(4) outperformed all other methods, as expected for a higher-order approach. Overall, UCC-based self-consistent electron propagator theory offers a promising framework for developing higher-order and non-perturbative Hermitian methods for IP and EA calculations. Future work will focus on developing and implementing advanced commutator-truncation schemes – such as extended qUCCSD schemes (IP/EA-eqUCCSD)⁴⁴ and cubic UCCSD schemes (IP/EA-cUCCSD)⁴⁴ – to further improve accuracy and explore the limits of UCCSD-based self-consistent electron propagator theory.

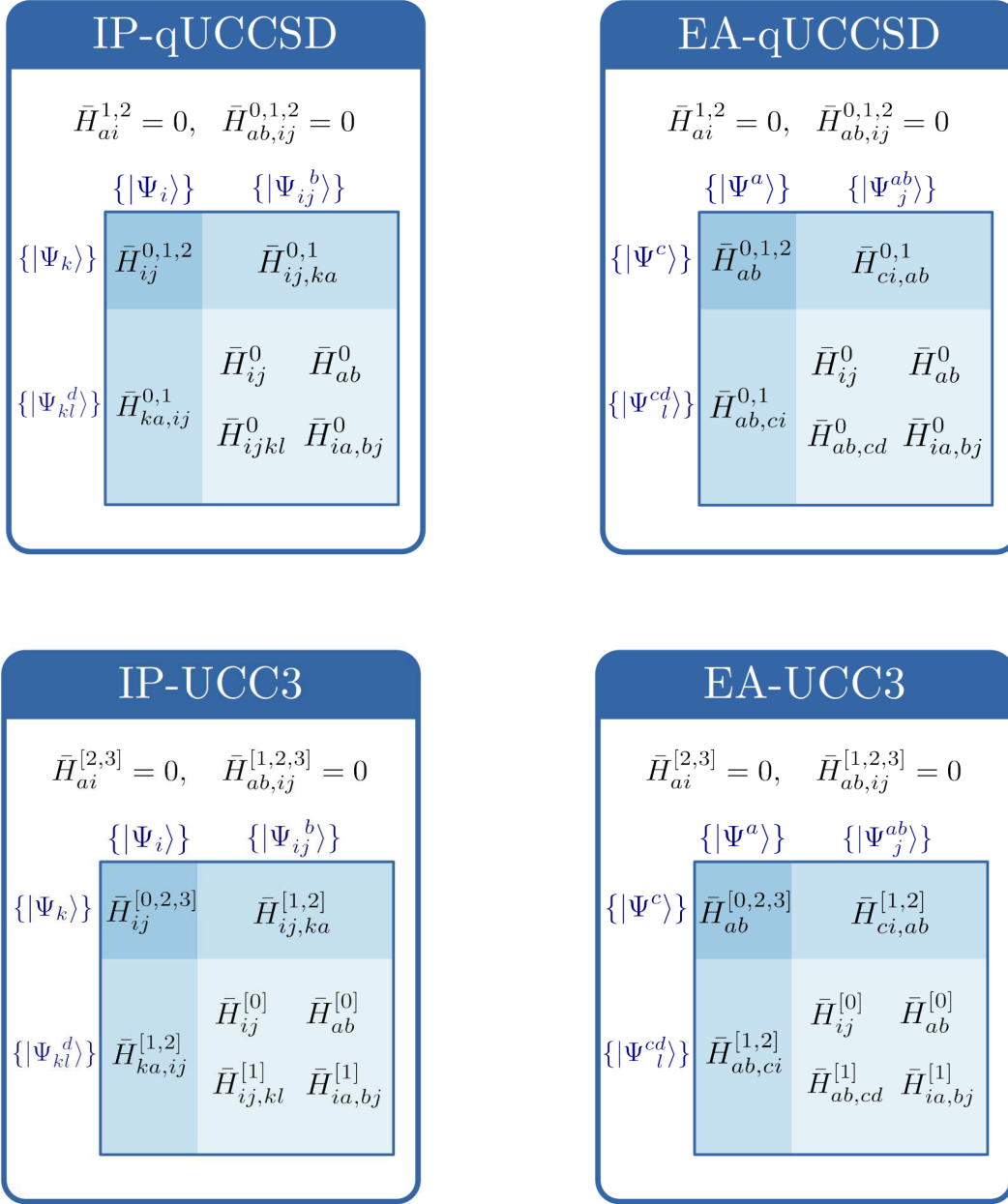


Figure 1: Block structure and constituent terms of the similarity-transformed Hamiltonian (\bar{H}) and amplitude equations in practical UCC-based electron propagator implementations. In the UCC3 scheme, the superscripts on \bar{H} denote the perturbation order to which both \bar{H} and the amplitude equations are expanded in each block. In the qUCCSD scheme, the superscripts instead indicate commutator rank, as defined in eq (34) -(38).

Table 1: Components of \bar{H} in the target-state eigenvalue equations for qUCCSD, IP-qUCCSD, and EA-qUCCSD.

qUCCSD	IP-qUCCSD	EA-qUCCSD
$\bar{H}_{SS}: \bar{H}_{ij}, \bar{H}_{ab}, \bar{H}_{ia,bj}$	$\bar{H}_{1h-1h}: \bar{H}_{ij}$	$\bar{H}_{1p-1p}: \bar{H}_{ab}$
$\bar{H}_{SD}: \bar{H}_{ci,ab}, \bar{H}_{ij,ka}, \bar{H}_{ibc,ajk}$	$\bar{H}_{1h-2h1p}: \bar{H}_{ij,ka}$	$\bar{H}_{1p-1h2p}: \bar{H}_{ci,ab}$
$\bar{H}_{DS}: \bar{H}_{ab,ci}, \bar{H}_{ka,ij}, \bar{H}_{ajk,ibc}$	$\bar{H}_{2h1p-1h}: \bar{H}_{ka,ij}$	$\bar{H}_{1h2p-1p}: \bar{H}_{ab,ci}$
$\bar{H}_{DD}: \bar{H}_{ij}, \bar{H}_{ab}, \bar{H}_{ia,bj}, \bar{H}_{ij,kl}, \bar{H}_{ab,cd}$	$\bar{H}_{2h1p-2h1p}: \bar{H}_{ij}, \bar{H}_{ab}, \bar{H}_{ia,bj}, \bar{H}_{ij,kl}$	$\bar{H}_{1h2p-1h2p}: \bar{H}_{ij}, \bar{H}_{ab}, \bar{H}_{ia,bj}, \bar{H}_{ab,cd}$

Table 2: Statistical deviations (eV) for 25 1h-dominated vertical ionization potentials computed with IP-EOM-CCSD, IP-ADC(3), IP-ADC(4), IP-UCC3, and IP-qUCCSD relative to FCI reference data^a. All systems have closed-shell reference states.

Method	MD	MAD	SD	MaxD(+)	MinD(-)
IP-EOM-CCSD	0.03	0.11	0.13	0.27	-0.24
IP-ADC(3)	0.26	0.31	0.29	0.84	-0.19
IP-ADC(4) ^b	-0.25	0.27	0.27	0.09	-0.84
IP-UCC3	0.27	0.27	0.18	0.61	-0.05
IP-qUCCSD	0.18	0.19	0.13	0.46	-0.09

^a “MD”, “MAD”, “SD”, “MaxD(+)”, and “MinD(-)” denote the mean deviation, mean absolute deviation, standard deviation, maximum positive deviation, and minimum negative deviation, respectively, relative to the FCI or CISDTQ reference values reported in ref. 75.

^b Ref. 77.

Table 3: Statistical deviations (eV) for 201 1h-dominated vertical ionization potentials computed with IP-EOM-CCSD, IP-ADC(3), IP-ADC(4), IP-UCC3, and IP-qUCCSD relative to IP-EOM-CCSDT reference values in the CGB dataset^a. All systems have closed-shell reference states.

Method	MD	MAD	SD	MaxD(+)	MinD(-)
IP-EOM-CCSD	0.19	0.24	0.28	0.89	-2.52
IP-ADC(3)	0.27	0.35	0.35	1.29	-0.83
IP-ADC(4) ^b	-0.25	0.27	0.27	0.17	-1.44
IP-UCC3	0.26	0.30	0.27	0.99	-0.83
IP-qUCCSD	0.18	0.23	0.22	1.00	-0.63

^a “MD”, “MAD”, “SD”, “MaxD(+)”, and “MinD(-)” denote the mean deviation, mean absolute deviation, standard deviation, maximum positive deviation, and minimum negative deviation, respectively, relative to the IP-EOM-CCSDT reference values reported in ref. [163](#).

^b Ref. [77](#).

Table 4: Statistical deviations (eV) for 17 1h-dominated vertical ionization potentials computed with IP-EOM-CCSD, IP-ADC(3), IP-ADC(4), IP-UCC3, and IP-qUCCSD relative to FCI reference data^a. All systems have open-shell reference states.

Method	MD	MAD	SD	MaxD(+)	MinD(-)
IP-EOM-CCSD	0.04	0.16	0.22	0.34	-0.63
IP-ADC(3)	0.12	0.24	0.34	0.91	-0.63
IP-ADC(4) ^b	-0.16	0.16	0.20	0.03	-0.63
IP-UCC3	0.11	0.20	0.26	0.58	-0.54
IP-qUCCSD	0.06	0.18	0.23	0.44	-0.58

^a “MD”, “MAD”, “SD”, “MaxD(+)”, and “MinD(-)” denote the mean deviation, mean absolute deviation, standard deviation, maximum positive deviation and minimum negative deviation, respectively, relative to the FCI or CISDTQ reference values reported in ref. [75](#).

^b Ref. [77](#).

Table 5: Statistical deviations (eV) for 35 1p-dominated vertical electron affinities computed with EA-EOM-CCSD, EA-ADC(3), EA-ADC(4), EA-UCC3, and EA-qUCCSD relative to FCI reference data^a. All systems have closed-shell reference states.

Method	MD	MAD	SD	MaxD(+)	MinD(-)
EA-EOM-CCSD	0.01	0.06	0.11	0.48	-0.21
EA-ADC(3)	0.03	0.05	0.09	0.37	-0.07
EA-ADC(4) ^b	0.04	0.05	0.10	0.50	-0.03
EA-UCC3	0.01	0.05	0.10	0.41	-0.12
EA-qUCCSD	0.01	0.05	0.10	0.42	-0.12

^a “MD”, “MAD”, “SD”, “MaxD(+)”, and “MinD(-)” denote the mean deviation, mean absolute deviation, standard deviation, maximum positive deviation and minimum negative deviation, respectively, relative to the FCI or CISDTQ reference values reported in ref. 76.

^b Ref. 77.

Table 6: Statistical deviations (eV) for 16 1p-dominated vertical electron affinities computed with EA-EOM-CCSD, EA-ADC(3), EA-ADC(4), EA-UCC3, and EA-qUCCSD relative to FCI reference data^a. All systems have open-shell reference states.

Method	MD	MAD	SD	MaxD(+)	MinD(-)
EA-EOM-CCSD	-0.04	0.08	0.12	0.24	-0.29
EA-ADC(3)	-0.13	0.17	0.22	0.16	-0.59
EA-ADC(4) ^b	0.01	0.03	0.06	0.16	-0.15
EA-UCC3	-0.15	0.20	0.28	0.36	-0.79
EA-qUCCSD	-0.13	0.17	0.24	0.30	-0.68

^a “MD”, “MAD”, “SD”, “MaxD(+)”, and “MinD(-)” denote the mean deviation, mean absolute deviation, standard deviation, maximum positive deviation and minimum negative deviation, respectively, relative to the FCI or CISDTQ reference values reported in Ref. 76.

^b Ref. 77.

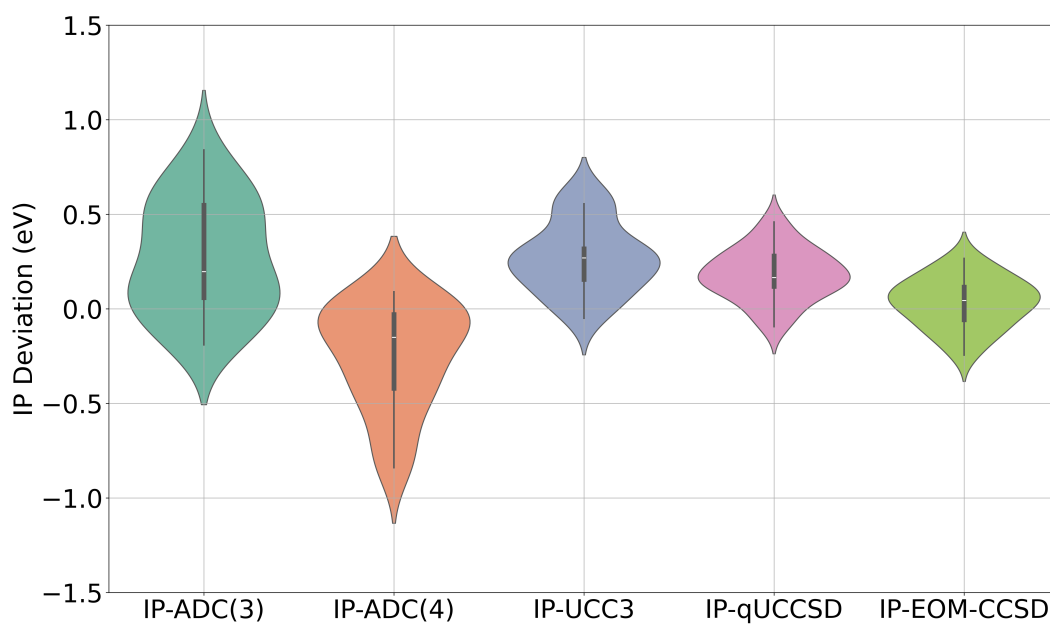


Figure 2: Violin plot of 25 1h-dominated vertical ionization potentials obtained for systems with closed-shell reference.

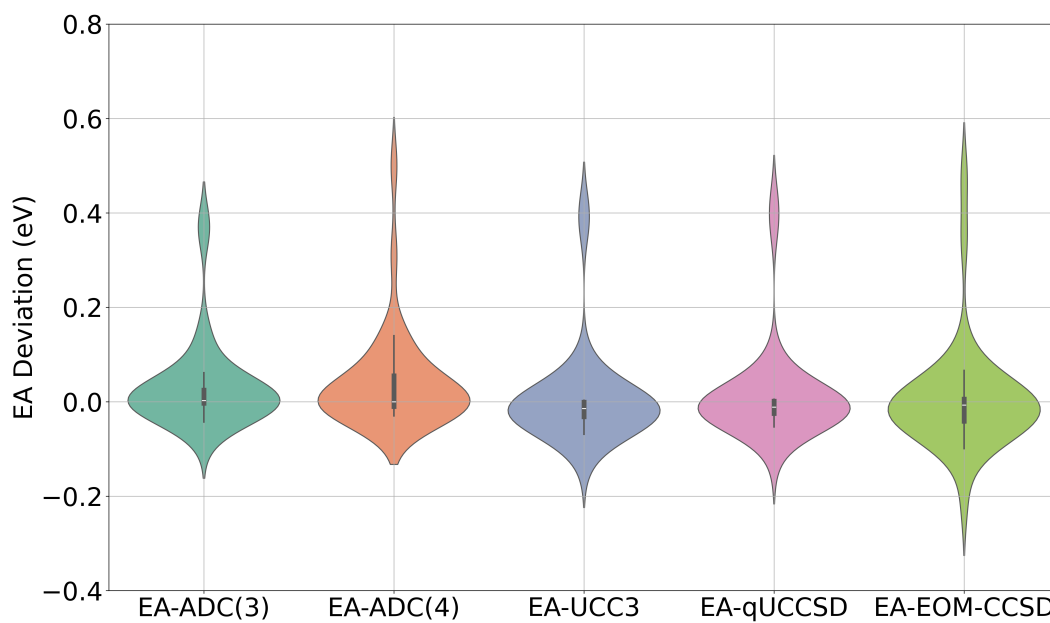


Figure 3: Violin plot of 35 1p-dominated vertical electron affinities obtained for systems with closed-shell reference.

Appendix: The ground-state energy expressions and amplitude equations of the qUCCSD method

In the qUCCSD method, the ground-state energy $E_{\text{gr}}^{\text{qUCCSD}}$ includes fully contracted terms of \bar{H} up to the third commutators and can be expressed as follows:

$$E_{\text{gr}}^{\text{qUCCSD}} = E_{\text{HF}} + \langle \Phi_0 | \bar{H}^1 | \Phi_0 \rangle + \langle \Phi_0 | \bar{H}^2 | \Phi_0 \rangle + \langle \Phi_0 | \bar{H}^3 | \Phi_0 \rangle, \quad (1)$$

$$\langle \Phi_0 | \bar{H}^1 | \Phi_0 \rangle = \sum_{ijab} \frac{1}{8} \langle ij || ab \rangle \sigma_{ij}^{ab} + h.c., \quad (2)$$

$$\langle \Phi_0 | \bar{H}^2 | \Phi_0 \rangle = \sum_{ijab} \frac{1}{12} \langle ij || ab \rangle \sigma_i^a \sigma_j^b + h.c., \quad (3)$$

$$\begin{aligned} \langle \Phi_0 | \bar{H}^3 | \Phi_0 \rangle = & \left(\left(- \sum_{ijklabcd} \frac{1}{12} (\sigma_{kl}^{cd})^* \langle ij || ab \rangle \sigma_{ik}^{ac} \sigma_{jl}^{bd} + \sum_{ijklabcd} \frac{1}{24} (\sigma_{kl}^{cd})^* \langle ij || ab \rangle \sigma_{ij}^{ac} \sigma_{kl}^{bd} \right. \right. \\ & + \sum_{ijklabcd} \frac{1}{24} (\sigma_{kl}^{cd})^* \langle ij || ab \rangle \sigma_{ik}^{ab} \sigma_{jl}^{cd} - \sum_{ijklabcd} \frac{1}{96} (\sigma_{kl}^{cd})^* \langle ij || ab \rangle \sigma_{ij}^{cd} \sigma_{kl}^{ab} \left. \right) + h.c. \Big) \\ & + \left(\left(\sum_{ijklabc} \frac{1}{4} (\sigma_{jl}^{bc})^* \langle ij || ak \rangle \sigma_i^a \sigma_{kl}^{bc} - \sum_{ijkabcd} \frac{1}{4} (\sigma_{jk}^{cd})^* \langle ic || ab \rangle \sigma_i^a \sigma_{jk}^{bd} \right. \right. \\ & + \sum_{ijklabc} \frac{1}{2} (\sigma_{il}^{bc})^* \langle kj || ai \rangle \sigma_j^b \sigma_{lk}^{ca} - \sum_{ijkabcd} \frac{1}{2} (\sigma_{jk}^{cd})^* \langle ic || ab \rangle \sigma_j^b \sigma_{ik}^{ad} \\ & + \sum_{ijklabc} \frac{1}{12} (\sigma_{il}^{bc})^* \langle jk || ia \rangle \sigma_l^c \sigma_{kj}^{ab} - \sum_{ijkabcd} \frac{1}{12} (\sigma_{jk}^{cd})^* \langle ic || ab \rangle \sigma_k^d \sigma_{ij}^{ba} \\ & - \sum_{ijklabc} \frac{1}{8} (\sigma_{il}^{cb})^* \langle kj || ia \rangle \sigma_l^a \sigma_{kj}^{cb} + \sum_{ijkabcd} \frac{1}{8} (\sigma_{jk}^{dc})^* \langle ci || ab \rangle \sigma_i^d \sigma_{kj}^{ab} \left. \right) + h.c. \Big) \\ & + \left(\left(- \sum_{ijkabc} \frac{1}{12} (\sigma_k^c)^* \langle ij || ab \rangle \sigma_i^a \sigma_{jk}^{bc} + \sum_{ijkabc} \frac{1}{12} (\sigma_k^c)^* \langle ij || ab \rangle \sigma_i^c \sigma_{jk}^{ba} \right. \right. \\ & + \sum_{ijkabc} \frac{1}{12} (\sigma_k^c)^* \langle ij || ab \rangle \sigma_k^a \sigma_{ij}^{cb} + \sum_{ijkabc} \frac{1}{3} (\sigma_{ik}^{bc})^* \langle jb || ai \rangle \sigma_j^c \sigma_i^a \\ & - \sum_{ijklab} \frac{1}{12} (\sigma_{ij}^{ab})^* \langle kl || ij \rangle \sigma_k^a \sigma_l^b - \sum_{ijabcd} \frac{1}{12} (\sigma_{ij}^{cd})^* \langle cd || ab \rangle \sigma_j^b \sigma_i^a \left. \right) + h.c. \Big) \\ & + \left(\left(\sum_{ijkab} \frac{1}{3} (\sigma_k^b)^* \langle ij || ak \rangle \sigma_i^a \sigma_j^b - \sum_{ijabc} \frac{1}{3} (\sigma_j^a)^* \langle ai || bc \rangle \sigma_j^b \sigma_i^c \right) + h.c. \right). \quad (4) \end{aligned}$$

The qUCCSD ground-state amplitude equations are equivalent to $\bar{H}_{ai} = 0$ and $\bar{H}_{ab,ij} = 0$. Accordingly, \bar{H}_{ai} consists of all contributions from the single-commutator and double-commutator terms,

$$\bar{H}_{ai}^{\text{qUCCSD}} = \bar{H}_{ai}^1 + \bar{H}_{ai}^2 = 0. \quad (5)$$

$$\bar{H}_{ai}^1 = \sum_b f_{ab} t_i^b - \sum_j t_j^a f_{ji} + \frac{1}{2} \sum_{jbc} \langle aj || cb \rangle \sigma_{ij}^{cb} - \frac{1}{2} \sum_{jkb} \langle kj || ib \rangle \sigma_{jk}^{ba} + \sum_{jb} \langle aj || ib \rangle \sigma_j^b + \frac{1}{2} \sum_{jb} (\sigma_j^b)^* \langle ab || ij \rangle, \quad (6)$$

$$\begin{aligned} \bar{H}_{ai}^2 = & - \sum_{jklbc} \frac{1}{2} (\sigma_{jk}^{bc})^* \langle al || ik \rangle \sigma_{jl}^{bc} + \sum_{jkbcd} \frac{1}{2} (\sigma_{jk}^{bd})^* \langle ad || ic \rangle \sigma_{jk}^{bc} - \sum_{jklbc} (\sigma_{jk}^{bc})^* \langle bl || ji \rangle \sigma_{kl}^{ca} \\ & + \sum_{jkbcd} (\sigma_{jk}^{bc})^* \langle ab || dj \rangle \sigma_{ki}^{cd} - \sum_{jklbc} \frac{1}{4} (\sigma_{jk}^{bc})^* \langle bl || jk \rangle \sigma_{il}^{ac} + \sum_{jkbcd} \frac{1}{4} (\sigma_{jk}^{bd})^* \langle bd || jc \rangle \sigma_{ik}^{ac} \\ & + \sum_{jklbc} \frac{1}{4} (\sigma_{jk}^{bd})^* \langle bd || ic \rangle \sigma_{jk}^{ca} - \sum_{jkbcd} \frac{1}{4} (\sigma_{jk}^{bc})^* \langle al || jk \rangle \sigma_{il}^{cb} + \sum_{jkbce} \frac{5}{12} \langle jk || bc \rangle \sigma_j^b \sigma_{ik}^{ac} \\ & - \sum_{jkbce} \frac{1}{3} \langle jk || bc \rangle \sigma_k^a \sigma_{ij}^{cb} - \sum_{jkbce} \frac{1}{3} \langle jk || bc \rangle \sigma_i^c \sigma_{jk}^{ba} - \sum_{jkbce} \frac{1}{2} (\sigma_k^c)^* \langle cj || ib \rangle \sigma_{jk}^{ba} \\ & - \sum_{jkbce} \frac{1}{2} (\sigma_k^c)^* \langle aj || kb \rangle \sigma_{ij}^{cb} - \sum_{jkbce} \frac{1}{3} (\sigma_{jk}^{cb})^* \langle ab || ij \rangle \sigma_k^c - \sum_{jkbce} \frac{1}{6} (\sigma_{jk}^{bc})^* \langle bc || ji \rangle \sigma_k^a \\ & - \sum_{jkbce} \frac{1}{6} (\sigma_{jk}^{bc})^* \langle ab || kj \rangle \sigma_i^c + \sum_{jbcde} \frac{1}{4} (\sigma_j^c)^* \langle ac || bd \rangle \sigma_{ij}^{bd} + \sum_{jklb} \frac{1}{4} (\sigma_k^b)^* \langle jl || ik \rangle \sigma_{jl}^{ab} \\ & + \sum_{jbc} \langle aj || cb \rangle \sigma_j^b \sigma_i^c - \sum_{jkb} \langle kj || ib \rangle \sigma_j^b \sigma_k^a + \sum_{jbc} \frac{1}{2} (\sigma_j^b)^* \langle ab || cj \rangle \sigma_i^c - \sum_{jkb} \frac{1}{2} (\sigma_j^b)^* \langle kb || ij \rangle \sigma_k^a \\ & + \sum_{jbc} \frac{1}{2} (\sigma_j^c)^* \langle ac || ib \rangle \sigma_j^b - \sum_{jkb} \frac{1}{2} (\sigma_j^b)^* \langle ak || ij \rangle \sigma_k^b. \end{aligned} \quad (7)$$

The $\bar{H}_{ab,ij}$ contains all terms from the bare Hamiltonian up to the double-commutator,

$$\bar{H}_{ab,ij}^{\text{qUCCSD}} = \bar{H}_{ab,ij}^0 + \bar{H}_{ab,ij}^1 + \bar{H}_{ab,ij}^2 = 0. \quad (8)$$

$$\bar{H}_{ab,ij}^0 = \langle ab || ij \rangle, \quad (9)$$

$$\begin{aligned}\bar{H}_{ab,ij}^1 = & \sum_c f_{ac} \sigma_{ij}^{cb} - \sum_k f_{ki} \sigma_{kj}^{ab} + \sum_{kl} \frac{1}{2} \langle kl || ij \rangle \sigma_{kl}^{ab} + \sum_{cd} \frac{1}{2} \langle ab || cd \rangle \sigma_{ij}^{cd} + P(ij)P(ab) \sum_{kc} \langle ak || ic \rangle \sigma_{jk}^{bc} \\ & - P(ab) \sum_k \langle ka || ji \rangle \sigma_k^b + P(ij) \sum_c \langle ab || ic \rangle \sigma_j^c,\end{aligned}\quad (10)$$

$$\begin{aligned}\bar{H}_{ab,ij}^2 = & P(ij)P(ab) \sum_{klcd} \frac{1}{3} \langle kl || cd \rangle \sigma_{ik}^{ac} \sigma_{jl}^{bd} + \sum_{klcd} \frac{1}{6} \langle kl || cd \rangle \sigma_{ij}^{cd} \sigma_{kl}^{ab} - P(ab) \sum_{klcd} \frac{1}{3} \langle kl || cd \rangle \sigma_{ij}^{ad} \sigma_{kl}^{cb} \\ & - P(ij) \sum_{klcd} \frac{1}{3} \langle kl || cd \rangle \sigma_{il}^{ab} \sigma_{jk}^{dc} + P(ij)P(ab) \sum_{klcd} \frac{1}{3} (\sigma_{kl}^{cd})^* \langle ad || il \rangle \sigma_{jk}^{bc} + \sum_{klcd} \frac{1}{12} (\sigma_{kl}^{cd})^* \langle cd || ij \rangle \sigma_{kl}^{ab} \\ & + \sum_{klcd} \frac{1}{12} (\sigma_{kl}^{cd})^* \langle ab || kl \rangle \sigma_{ij}^{cd} - P(ab) \sum_{klcd} \frac{1}{6} (\sigma_{kl}^{cd})^* \langle ad || ij \rangle \sigma_{kl}^{cb} - P(ij) \sum_{klcd} \frac{1}{6} (\sigma_{kl}^{cd})^* \langle ab || il \rangle \sigma_{jk}^{dc} \\ & - P(ab) \sum_{klcd} \frac{1}{6} (\sigma_{kl}^{cd})^* \langle cb || kl \rangle \sigma_{ij}^{ad} - P(ij) \sum_{klcd} \frac{1}{6} (\sigma_{kl}^{cd})^* \langle cd || kj \rangle \sigma_{il}^{ab} - P(ij) \sum_{klc} (\sigma_l^c)^* \langle ck || lj \rangle \sigma_{ik}^{ab} \\ & + P(ab) \sum_{lcd} (\sigma_l^c)^* \langle bc || dl \rangle \sigma_{ij}^{ad} + P(ij) \sum_{lcd} \frac{1}{2} (\sigma_l^c)^* \langle ab || id \rangle \sigma_{jl}^{dc} - P(ab) \sum_{klc} \frac{1}{2} (\sigma_l^c)^* \langle ak || ij \rangle \sigma_{kl}^{bc} \\ & + \sum_{klc} (\sigma_l^c)^* \langle ck || ji \rangle \sigma_{kl}^{ab} + P(ij)P(ab) \sum_{klc} (\sigma_l^c)^* \langle bk || li \rangle \sigma_{jk}^{ca} - P(ij)P(ab) \sum_{lcd} (\sigma_l^c)^* \langle ac || dj \rangle \sigma_{il}^{db} \\ & - \sum_{lcd} (\sigma_l^c)^* \langle ab || dl \rangle \sigma_{ij}^{dc} - P(ij) \sum_{klc} \langle kl || cj \rangle \sigma_k^c \sigma_{il}^{ab} + P(ab) \sum_{kcd} \langle kb || cd \rangle \sigma_k^c \sigma_{ij}^{ad} \\ & - P(ij)P(ab) \sum_{klc} \langle kl || cj \rangle \sigma_l^b \sigma_{ik}^{ac} + P(ij)P(ab) \sum_{kcd} \langle kb || cd \rangle \sigma_j^d \sigma_{ik}^{ac} + P(ij) \sum_{klc} \frac{1}{2} \langle kl || ci \rangle \sigma_j^c \sigma_{kl}^{ba} \\ & - P(ab) \sum_{kcd} \frac{1}{2} \langle ka || cd \rangle \sigma_k^b \sigma_{ij}^{dc} + P(ab) \sum_{kl} \frac{1}{2} \langle kl || ij \rangle \sigma_k^a \sigma_l^b - P(ij)P(ab) \sum_{kc} \langle ak || cj \rangle \sigma_i^c \sigma_k^b \\ & + P(ij) \sum_{cd} \frac{1}{2} \langle ab || cd \rangle \sigma_i^c \sigma_j^d - P(ab) \sum_{kc} \frac{1}{3} (\sigma_k^c)^* \langle ac || ij \rangle \sigma_k^b - P(ij) \sum_{kc} \frac{1}{3} (\sigma_k^c)^* \langle ab || ik \rangle \sigma_j^c.\end{aligned}\quad (11)$$

Supporting Information Available

See the Supporting Information for computational details (molecular geometries and basis sets) and for complete lists of individual VIPs and VEAs for the five benchmark datasets computed with IP/EA-UCC3 and IP/EA-qUCCSD.

Note

The authors declare no conflict of interest with regard to this content.

Acknowledgement

This work has been supported by the National Natural Science Foundation of China (Grant No. 22173005) and Fundamental Research Funds for the Central Universities (FRF-BR-23-02B). J. L. is grateful to Prof. Lan Cheng at Johns Hopkins University for helpful discussions and useful suggestions for revising the manuscript and support.

References

- (1) (a) Linderberg, J.; Öhrn, Y. *Propagators in Quantum Chemistry*, 1st ed.; Academic Press: New York, 1973; (b) Linderberg, J.; Öhrn, Y. *Propagators in Quantum Chemistry*, 2nd ed.; John Wiley & Sons: New Jersey, 2004.
- (2) Pickup, B.; Goscinski, O. Direct calculation of ionization energies. *Mol. Phys.* **1973**, *26*, 1013–1035.
- (3) Cederbaum, L. S. One-body Green's function for atoms and molecules: theory and application. *J. Phys. B: At. Mol. Phys.* **1975**, *8*, 290–303.
- (4) Cederbaum, L. S.; Domcke, W. Theoretical Aspects of Ionization Potentials and Photoelectron Spectroscopy: A Green's Function Approach. *Adv. Chem. Phys.* **1977**, *36*, 205–344.
- (5) Oddershede, J. In *Advances in Chemical Physics*; Lawley, K. P., Ed.; Propagator Methods; John Wiley & Sons, Ltd, 1987; Chapter 3, pp 201–239.

- (6) Goscinski, O.; Weiner, B. The Role of Algebraic Formulations of Approximate Green's Functions for Systems With a Finite Number of Electrons. *Phys. Scr.* **1980**, *21*, 385–393.
- (7) Jørgensen, P.; Simon, J. *Second Quantization-Based Methods in Quantum Chemistry*; Academic Press: New York, 1981.
- (8) Schirmer, J. Beyond the random-phase approximation: A new approximation scheme for the polarization propagator. *Phys. Rev. A* **1982**, *26*, 2395–2416.
- (9) Schirmer, J.; Cederbaum, L. S.; Walter, O. New approach to the one-particle Green's function for finite Fermi systems. *Phys. Rev. A* **1983**, *28*, 1237–1259.
- (10) Oddershede, J.; Jørgensen, P.; Yeager, D. L. *Polarization propagator methods in atomic and molecular calculations*; 1984; Vol. 2; pp 33–92.
- (11) Kutzelnigg, W.; Mukherjee, D. Time-independent theory of one-particle Green's functions. *J. Chem. Phys.* **1989**, *90*, 5578–5594.
- (12) Longo, R.; Champagne, B.; Öhrn, Y. Electron propagator theory and application. *Theor. Chim. Acta.* **1995**, *90*, 397–419.
- (13) Simons, J. Response of a Molecule to Adding or Removing an Electron. *Adv. Quantum Chem.* **2005**, *50*, 213–233.
- (14) Danovich, D. Green's function methods for calculating ionization potentials, electron affinities, and excitation energies. *WIREs Comput Mol Sci* **2011**, *1*, 377–387.
- (15) Ortiz, J. V. Electron propagator theory: an approach to prediction and interpretation in quantum chemistry. *WIREs Comput Mol Sci* **2012**, *3*, 123–142.
- (16) Schirmer, J. *Many-body Methods for Atoms, Molecules and Clusters*; Lecture Notes in Chemistry; Springer: Switzerland, 2018; Vol. 94.

- (17) Oddershede, J. Polarization propagator calculations. *Adv. Quantum Chem.* **1978**, *11*, 275–352.
- (18) Bak, K. L.; Koch, H.; Oddershede, J.; Christiansen, O.; Sauer, S. P. A. Atomic integral driven second order polarization propagator calculations of the excitation spectra of naphthalene and anthracene. *J. Chem. Phys.* **2000**, *112*, 4173–4185.
- (19) Faleev, S. V.; van Schilfgaarde, M.; Kotani, T. All-electron self-consistent *GW* approximation: application to Si, MnO, and NiO. *Phys. Rev. Lett.* **2004**, *93*, 126406.
- (20) van Schilfgaarde, M.; Kotani, T.; Faleev, S. V. Quasiparticle self-consistent *GW* theory. *Phys. Rev. Lett.* **2006**, *96*, 226402.
- (21) van Setten, M. J.; Weigend, F.; Evers, F. The *GW*-method for quantum chemistry applications: theory and implementation. *J. Chem. Theory Comput.* **2013**, *9*, 232–246.
- (22) Reining, L. The *GW* approximation: content, successes and limitations. *WIREs Comput. Mol. Sci.* **2018**, *8*, e1344.
- (23) Geertsen, J.; Oddershede, J.; Scuseria, G. E. Calculation of spectra and spin–spin coupling constants using a coupled–cluster polarization propagator method. *Int. J. Quantum Chem.* **1987**, *32*, 475–485.
- (24) Kowalski, K.; Bhaskaran-Nair, K.; Shelton, W. A. Coupled-cluster representation of Green function employing modified spectral resolutions of similarity transformed Hamiltonians. *J. Chem. Phys.* **2014**, *141*, 094102.
- (25) Vila, F. D.; Kas, J. J.; Rehr, J. J.; Kowalski, K.; Peng, B. Equation-of-motion coupled-cluster cumulant Green’s function for excited states and X-Ray spectra. *Front. Chem.* **2021**, *9*, 734945.

- (26) Peng, B.; Bauman, N. P.; Gulania, S.; Kowalski, K. In *Annual Reports in Computational Chemistry*; Dixon, D. A., Ed.; Chapter Two - Coupled cluster Green's function: Past, present, and future; Elsevier, 2021; Vol. 17; Chapter 2, pp 23–53.
- (27) Salpeter, E. E.; Bethe, H. A. A Relativistic Equation for Bound-State Problems. *Phys. Rev.* **1951**, *84*, 1232–1242.
- (28) Strinati, G. Application of the Green's functions method to the study of the optical properties of semiconductors. *Riv. Nuovo Cim.* **1988**, *11*, 1–86.
- (29) Blase, X.; Duchemin, I.; Jacquemin, D.; Loos, P.-F. The Bethe–Salpeter Equation Formalism: From Physics to Chemistry. *J. Phys. Chem. Lett.* **2020**, *11*, 7371–7382.
- (30) Schirmer, J. Closed-form intermediate representations of many-body propagators and resolvent matrices. *Phys. Rev. A* **1991**, *43*, 4647–4659.
- (31) Trofimov, A. B.; Schirmer, J. An efficient polarization propagator approach to valence electron excitation spectra. *J. Phys. B: At. Mol. Opt. Phys.* **1995**, *28*, 2299–2324.
- (32) Mertins, F.; Schirmer, J. Algebraic propagator approaches and intermediate-state representations. I. The biorthogonal and unitary coupled-cluster methods. *Phys. Rev. A* **1996**, *53*, 2140–2152.
- (33) Trofimov, A. B.; Stelter, G.; Schirmer, J. A consistent third-order propagator method for electronic excitation. *J. Chem. Phys.* **1999**, *111*, 9982–9999.
- (34) Trofimov, A. B.; Stelter, G.; Schirmer, J. Electron excitation energies using a consistent third-order propagator approach: Comparison with full configuration interaction and coupled cluster results. *J. Chem. Phys.* **2002**, *117*, 6402–6410.
- (35) Schirmer, J.; Trofimov, A. B. Intermediate state representation approach to physical properties of electronically excited molecules. *J. Chem. Phys.* **2004**, *120*, 11449–11464.

- (36) Starcke, J. H.; Wormit, M.; Dreuw, A. Unrestricted algebraic diagrammatic construction scheme of second order for the calculation of excited states of medium-sized and large molecules. *J. Chem. Phys.* **2009**, *130*, 024104.
- (37) Dreuw, A.; Wormit, M. The algebraic diagrammatic construction scheme for the polarization propagator for the calculation of excited states. *WIREs Comput. Mol. Sci.* **2015**, *5*, 82–95.
- (38) Leitner, J.; Dempwolff, A. L.; Dreuw, A. The fourth-order algebraic diagrammatic construction scheme for the polarization propagator. *J. Chem. Phys.* **2022**, *157*, 184101.
- (39) Sokolov, A. Y. Multi-reference algebraic diagrammatic construction theory for excited states: General formulation and first-order implementation. *J. Chem. Phys.* **2018**, *149*, 204113.
- (40) Mazin, I. M.; Sokolov, A. Y. Multireference Algebraic Diagrammatic Construction Theory for Excited States: Extended Second-Order Implementation and Benchmark. *J. Chem. Theory Comput.* **2021**, *17*, 6152–6165.
- (41) Chakraborty, S.; Mukhopadhyay, T.; Nayak, M. K.; Dutta, A. K. A relativistic third-order algebraic diagrammatic construction theory for electron detachment, attachment, and excitation problems. *J. Chem. Phys.* **2025**, *162*, 104106.
- (42) Liu, J.; Asthana, A.; Cheng, L.; Mukherjee, D. Unitary coupled-cluster based self-consistent polarization propagator theory: A third-order formulation and pilot applications. *J. Chem. Phys.* **2018**, *148*, 24110.
- (43) Liu, J.; Cheng, L. Unitary coupled-cluster based self-consistent polarization propagator theory: A quadratic unitary coupled-cluster singles and doubles scheme. *J. Chem. Phys.* **2021**, *155*, 174102.

- (44) Liu, J.; Matthews, D. A.; Cheng, L. Quadratic Unitary Coupled-Cluster Singles and Doubles Scheme: Efficient Implementation, Benchmark Study, and Formulation of an Extended Version. *J. Chem. Theory Comput.* **2022**, *18*, 2281–2291.
- (45) Yu, H.; Zhang, Y.; Liu, J. Benchmark Calculations of Vertical Excitation Energies for Medium-sized Molecules using Unitary Coupled-Cluster based Polarization Propagator Theory. *J. Chem. Phys. A* **2025**, *129*, 6459–6469.
- (46) Hodecker, M.; Thielen, S. M.; Liu, J.; Rehn, D. R.; Dreuw, A. Third-Order Unitary Coupled Cluster (UCC3) for Excited Electronic States: Efficient Implementation and Benchmarking. *J. Chem. Theory Comput.* **2020**, *16*, 3654–3663.
- (47) Hodecker, M.; Dreuw, A. Unitary coupled cluster ground- and excited-state molecular properties. *J. Chem. Phys.* **2020**, *153*, 084112.
- (48) Majee, K.; Chakraborty, S.; Mukhopadhyay, T.; Nayak, M. K.; Dutta, A. K. A reduced cost four-component relativistic unitary coupled cluster method for atoms and molecules. *J. Chem. Phys.* **2024**, *161*, 034101.
- (49) Hüfner, S. *Photoelectron spectroscopy: principles and applications*, 3rd ed.; Springer: Heidelberg, 2003.
- (50) van der Heide, P. *X-ray photoelectron spectroscopy: an introduction to principles and practices*; John Wiley & Sons, 2011.
- (51) Cederbaum, L.; Hohlneicher, G.; Peyerimhoff, S. Calculation of the vertical ionization potentials of formaldehyde by means of perturbation theory. *Chem. Phys. Lett.* **1971**, *11*, 421–424.
- (52) Doll, J. D.; Reinhardt, W. P. Many-Body Green’s Functions for Finite, Nonuniform Systems: Applications to Closed Shell Atoms. *J. Chem. Phys.* **1972**, *57*, 1169–1184.

- (53) Cederbaum, L. S. Direct calculation of ionization potentials of closed-shell atoms and molecules. *Theor. Chim. Acta* **1973**, *31*, 239–260.
- (54) Von Niessen, W.; Schirmer, J.; Cederbaum, L. Computational methods for the one-particle green's function. *Comput. Phys. Rep.* **1984**, *1*, 57–125.
- (55) Angonoa, G.; Walter, O.; Schirmer, J. Theoretical K-shell ionization spectra of N₂ and CO by a fourth-order Green's function method. *J. Chem. Phys.* **1987**, *87*, 6789–6801.
- (56) Schirmer, J.; Angonoa, G. On Green's function calculations of the static self-energy part, the ground state energy and expectation values. *J. Chem. Phys.* **1989**, *91*, 1754–1761.
- (57) Schirmer, J.; Cederbaum, L. S. The two-particle-hole Tamm-Dancoff approximation (2ph-TDA) equations for closed-shell atoms and molecules. *J. Phys. B: At. Mol. Phys.* **1978**, *11*, 1889.
- (58) Ortiz, J. V. Partial third-order quasiparticle theory: Comparisons for closed-shell ionization energies and an application to the Borazine photoelectron spectrum. *J. Chem. Phys.* **1996**, *104*, 7599–7605.
- (59) Opoku, E.; Pawłowski, F.; Ortiz, J. V. A new generation of diagonal self-energies for the calculation of electron removal energies. *J. Chem. Phys.* **2021**, *155*, 204107.
- (60) Ortiz, J. V. A nondiagonal, renormalized extension of partial third-order quasiparticle theory: Comparisons for closed-shell ionization energies. *J. Chem. Phys.* **1998**, *108*, 1008–1014.
- (61) Ortiz, J. V. An efficient, renormalized self-energy for calculating the electron binding energies of closed-shell molecules and anions. *Int. J. Quantum Chem.* **2005**, *105*, 803–808.

- (62) Opoku, E.; Pawłowski, F.; Ortiz, J. V. New-Generation Electron-Propagator Methods for Calculations of Electron Affinities and Ionization Energies: Tests on Organic Photovoltaic Molecules. *J. Chem. Theory Comput.* **2024**, *20*, 290–306.
- (63) Opoku, E.; Pawłowski, F.; Ortiz, J. V. New-Generation Electron-Propagator Methods for Molecular Electron-Binding Energies. *J. Phys. Chem. A* **2024**, *128*, 1399–1416.
- (64) Schirmer, J.; Trofimov, A. B.; Stelter, G. A non-Dyson third-order approximation scheme for the electron propagator. *J. Chem. Phys.* **1998**, *109*, 4734–4744.
- (65) Trofimov, A. B.; Schirmer, J. Molecular ionization energies and ground- and ionic-state properties using a non-Dyson electron propagator approach. *J. Chem. Phys.* **2005**, *123*, 144115.
- (66) Storchi, L.; Vitillaro, G.; Tarantelli, F. Implementation and use of a direct, partially integral-driven non-Dyson propagator method for molecular ionization. *J. Comput. Chem.* **2009**, *30*, 818–825.
- (67) Banerjee, S.; Sokolov, A. Y. Third-order algebraic diagrammatic construction theory for electron attachment and ionization energies: Conventional and Green’s function implementation. *J. Chem. Phys.* **2019**, *151*, 224112.
- (68) Banerjee, S.; Sokolov, A. Y. Non-Dyson Algebraic Diagrammatic Construction Theory for Charged Excitations in Solids. *J. Chem. Theory Comput.* **2022**, *18*, 5337–5348.
- (69) Banerjee, S.; Sokolov, A. Y. Algebraic Diagrammatic Construction Theory for Simulating Charged Excited States and Photoelectron Spectra. *J. Chem. Theory Comput.* **2023**, *19*, 3037–3053.
- (70) Dempwolff, A. L.; Schneider, M.; Hodecker, M.; Dreuw, A. Efficient implementation of the non-Dyson third-order algebraic diagrammatic construction approximation for

- the electron propagator for closed- and open-shell molecules. *J. Chem. Phys.* **2019**, *150*, 064108.
- (71) Schirmer, J.; Thiel, A. An intermediate state representation approach to K-shell ionization in molecules. I. Theory. *J. Chem. Phys.* **2001**, *115*, 10621–10635.
- (72) Thiel, A.; Schirmer, J.; Köppel, H. An intermediate state representation approach to K-shell ionization in molecules. II. Computational tests. *J. Chem. Phys.* **2003**, *119*, 2088–2101.
- (73) Schneider, M.; Soshnikov, D. Y.; Holland, D. M. P.; Powis, I.; Antonsson, E.; Patainen, M.; Nicolas, C.; Miron, C.; Wormit, M.; Dreuw, A.; Trofimov, A. B. A fresh look at the photoelectron spectrum of bromobenzene: A third-order non-Dyson electron propagator study. *J. Chem. Phys.* **2015**, *143*, 144103.
- (74) Dempwolff, A. L.; Paul, A. C.; Belogolova, A. M.; Trofimov, A. B.; Dreuw, A. Intermediate state representation approach to physical properties of molecular electron-detached states. I. Theory and implementation. *J. Chem. Phys.* **2020**, *152*, 024113.
- (75) Dempwolff, A. L.; Paul, A. C.; Belogolova, A. M.; Trofimov, A. B.; Dreuw, A. Intermediate state representation approach to physical properties of molecular electron-detached states. II. Benchmarking. *J. Chem. Phys.* **2020**, *152*, 024125.
- (76) Dempwolff, A. L.; Belogolova, A. M.; Trofimov, A. B.; Dreuw, A. Intermediate state representation approach to physical properties of molecular electron-attached states: Theory, implementation, and benchmarking. *J. Chem. Phys.* **2021**, *154*, 104117.
- (77) Leitner, J.; Dempwolff, A. L.; Dreuw, A. Fourth-Order Algebraic Diagrammatic Construction for Electron Detachment and Attachment: The IP- and EA-ADC(4) Methods. *J. Phys. Chem. A* **2024**, *128*, 7680–7690.

- (78) Banerjee, S.; Sokolov, A. Y. Efficient implementation of the single-reference algebraic diagrammatic construction theory for charged excitations: Applications to the TEMPO radical and DNA base pairs. *J. Chem. Phys.* **2021**, *154*, 074105.
- (79) Cheng-zheng, H. Green's functions in coupled-cluster form. *Commun. Theor. Phys.* **1990**, *13*, 287.
- (80) Nooijen, M.; Snijders, J. G. Coupled cluster approach to the single-particle Green's function. *Int. J. Quantum Chem.* **1992**, *44*, 55–83.
- (81) Nooijen, M.; Snijders, J. G. Coupled cluster Green's function method: Working equations and applications. *Int. J. Quantum Chem.* **1993**, *48*, 15–48.
- (82) Nooijen, M.; Snijders, J. G. Second order many-body perturbation approximations to the coupled cluster Green's function. *J. Chem. Phys.* **1995**, *102*, 1681–1688.
- (83) Meissner, L.; Bartlett, R. J. Electron propagator theory with the ground state correlated by the coupled-cluster method. *Int. J. Quantum Chem.* **1993**, *48*, 67–80.
- (84) Bhaskaran-Nair, K.; Kowalski, K.; Shelton, W. A. Coupled cluster Green function: Model involving single and double excitations. *J. Chem. Phys.* **2016**, *144*, 144101.
- (85) Peng, B.; Kowalski, K. Green's Function Coupled-Cluster Approach: Simulating Photoelectron Spectra for Realistic Molecular Systems. *J. Chem. Theory Comput.* **2018**, *14*, 4335–4352.
- (86) Nakatsuji, H.; Hirao, K. Cluster expansion of the wavefunction. Symmetry-adapted-cluster expansion, its variational determination, and extension of open-shell orbital theory. *J. Chem. Phys.* **1978**, *68*, 2053–2065.
- (87) Nakatsuji, N. Cluster expansion of the wavefunction. Excited states. *Chem. Phys. Lett.* **1978**, *59*, 362–364.

- (88) Nakatsuji, H. Cluster expansion of the wavefunction. Electron correlations in ground and excited states by SAC (symmetry-adapted-cluster) and SAC CI theories. *Chem. Phys. Lett.* **1979**, *67*, 329–333.
- (89) Nakatsuji, H.; Ohta, K.; Hirao, K. Cluster expansion of the wave function. Electron correlations in the ground state, valence and Rydberg excited states, ionized states, and electron attached states of formaldehyde by SAC and SAC–CI theories. *J. Chem. Phys.* **1981**, *75*, 2952–2958.
- (90) Nakajima, T.; Nakatsuji, H. Analytical energy gradient of the ground, excited, ionized and electron-attached states calculated by the SAC/SAC-CI method. *Chem. Phys. Lett.* **1997**, *280*, 79–84.
- (91) Sekino, H.; Bartlett, R. J. A linear response, coupled-cluster theory for excitation energy. *Int. J. Quantum Chem.* **1984**, *26*, 255–265.
- (92) Geertsens, J.; Rittby, M.; Bartlett, R. J. The equation-of-motion coupled-cluster method: Excitation energies of Be and CO. *Chem. Phys. Lett.* **1989**, *164*, 57–62.
- (93) Stanton, J. F.; Bartlett, R. J. The equation of motion coupled-cluster method. A systematic biorthogonal approach to molecular excitation energies, transition probabilities, and excited state properties. *J. Chem. Phys.* **1993**, *98*, 7029–7039.
- (94) Bartlett, R. J.; Stanton, J. F. In *Review of Computational Chemistry*; Lipkowitz, K. B., Boyd, D. B., Eds.; Applications of Post-Hartree–Fock Methods: A Tutorial; John Wiley & Sons, Ltd, 1994; pp 65–169.
- (95) Mertins, F.; Schirmer, J.; Tarantelli, A. Algebraic propagator approaches and intermediate-state representations. II. The equation-of-motion methods for N , $N\pm 1$, and $N\pm 2$ electrons. *Phys. Rev. A* **1996**, *53*, 2153–2168.

- (96) Kowalski, K.; Piecuch, P. The active-space equation-of-motion coupled-cluster methods for excited electronic states: The EOMCCSDt approach. *J. Chem. Phys.* **2000**, *113*, 8490–8502.
- (97) Kucharski, S. A.; Włoch, M.; Musiał, M.; Bartlett, R. J. Coupled-cluster theory for excited electronic states: The full equation-of-motion coupled-cluster single, double, and triple excitation method. *J. Chem. Phys.* **2001**, *115*, 8263–8266.
- (98) Hirata, S. Higher-order equation-of-motion coupled-cluster methods. *J. Chem. Phys.* **2004**, *121*, 51–59.
- (99) Kállay, M.; Gauss, J. Calculation of excited-state properties using general coupled-cluster and configuration-interaction models. *J. Chem. Phys.* **2004**, *121*, 9257–9269.
- (100) Levchenko, S. V.; Krylov, A. I. Equation-of-motion spin-flip coupled-cluster model with single and double substitutions: Theory and application to cyclobutadiene. *J. Chem. Phys.* **2004**, *120*, 175–185.
- (101) Matthews, D. A.; Stanton, J. F. A new approach to approximate equation-of-motion coupled cluster with triple excitations. *J. Chem. Phys.* **2016**, *145*, 124102.
- (102) Monkhorst, H. J. Calculation of properties with the coupled-cluster method. *Int. J. Quantum Chem.* **1977**, *12*, 421–432.
- (103) Mukherjee, D.; Mukherjee, P. A response-function approach to the direct calculation of the transition-energy in a multiple-cluster expansion formalism. *Chem. Phys.* **1979**, *39*, 325–335.
- (104) Ghosh, S.; Mukherjee, D.; Bhattacharyya, S. Application of linear response theory in a coupled cluster framework for the calculation of ionization potentials. *Mol. Phys.* **1981**, *43*, 173–179.

- (105) Emrich, K. An extension of the coupled cluster formalism to excited states. *Nucl. Phys. A* **1981**, *351*, 397–438.
- (106) Dalgaard, E.; Monkhorst, H. J. Some aspects of the time-dependent coupled-cluster approach to dynamic response functions. *Phys. Rev. A* **1983**, *28*, 1217–1222.
- (107) Koch, H.; Jørgensen, P. Coupled cluster response functions. *J. Chem. Phys.* **1990**, *93*, 3333–3344.
- (108) Koch, H.; Jensen, H. J. A.; Jørgensen, P.; Helgaker, T. Excitation energies from the coupled cluster singles and doubles linear response function (CCSDLR). Applications to Be, CH⁺, CO, and H₂O. *J. Chem. Phys.* **1990**, *93*, 3345–3350.
- (109) Christiansen, O.; Koch, H.; Jørgensen, P. Response functions in the CC3 iterative triple excitation model. *J. Chem. Phys.* **1995**, *103*, 7429–7441.
- (110) Krylov, A. I. Equation-of-Motion Coupled-Cluster Methods for Open-Shell and Electronically Excited Species: The Hitchhiker’s Guide to Fock Space. *Annu. Rev. Phys. Chem.* **2008**, *59*, 433–462.
- (111) Bartlett, R. J. Coupled-cluster theory and its equation-of-motion extensions. *WIREs Comput. Mol. Sci.* **2012**, *2*, 126–138.
- (112) Sneskov, K.; Christiansen, O. Excited state coupled cluster methods. *WIREs Comput. Mol. Sci.* **2012**, *2*, 566–584.
- (113) Loos, P.-F.; Scemama, A.; Jacquemin, D. The Quest for Highly Accurate Excitation Energies: A Computational Perspective. *J. Phys. Chem. Lett.* **2020**, *11*, 2374–2383.
- (114) Stanton, J. F.; Gauss, J. Analytic energy derivatives for ionized states described by the equation-of-motion coupled cluster method. *J. Chem. Phys.* **1994**, *101*, 8938–8944.
- (115) Nooijen, M.; Bartlett, R. J. Equation of motion coupled cluster method for electron attachment. *J. Chem. Phys.* **1995**, *102*, 3629–3647.

- (116) Stanton, J. F.; Gauss, J. A simple scheme for the direct calculation of ionization potentials with coupled-cluster theory that exploits established excitation energy methods. *J. Chem. Phys.* **1999**, *111*, 8785–8788.
- (117) Hirata, S.; Nooijen, M.; Bartlett, R. J. High-order determinantal equation-of-motion coupled-cluster calculations for ionized and electron-attached states. *Chem. Phys. Lett.* **2000**, *328*, 459–468.
- (118) Musiał, M.; Kucharski, S. A.; Bartlett, R. J. Equation-of-motion coupled cluster method with full inclusion of the connected triple excitations for ionized states: IP-EOM-CCSDT. *J. Chem. Phys.* **2003**, *118*, 1128–1136.
- (119) Musiał, M.; Bartlett, R. J. Equation-of-motion coupled cluster method with full inclusion of connected triple excitations for electron-attached states: EA-EOM-CCSDT. *J. Chem. Phys.* **2003**, *119*, 1901–1908.
- (120) Bomble, Y. J.; Saeh, J. C.; Stanton, J. F.; Szalay, P. G.; Kállay, M.; Gauss, J. Equation-of-motion coupled-cluster methods for ionized states with an approximate treatment of triple excitations. *J. Chem. Phys.* **2005**, *122*, 154107.
- (121) Gour, J. R.; Piecuch, P.; Włoch, M. Active-space equation-of-motion coupled-cluster methods for excited states of radicals and other open-shell systems: EA-EOMCCSDt and IP-EOMCCSDt. *J. Chem. Phys.* **2005**, *123*, 134113.
- (122) Kamiya, M.; Hirata, S. Higher-order equation-of-motion coupled-cluster methods for ionization processes. *J. Chem. Phys.* **2006**, *125*, 074111.
- (123) Kamiya, M.; Hirata, S. Higher-order equation-of-motion coupled-cluster methods for electron attachment. *J. Chem. Phys.* **2007**, *126*, 134112.
- (124) Stanton, J. F.; Gauss, J. Perturbative treatment of the similarity transformed Hamil-

- tonian in equation-of-motion coupled-cluster approximations. *J. Chem. Phys.* **1995**, *103*, 1064–1076.
- (125) Bozkaya, U. Accurate Electron Affinities from the Extended Koopmans’ Theorem Based on Orbital-Optimized Methods. *J. Chem. Theory Comput.* **2014**, *10*, 2041–2048.
- (126) Wälz, G.; Usvyat, D.; Korona, T.; Schütz, M. A hierarchy of local coupled cluster singles and doubles response methods for ionization potentials. *J. Chem. Phys.* **2016**, *144*, 084117.
- (127) Ma, F.; Wang, Z.; Guo, M.; Wang, F. Approximate equation-of-motion coupled-cluster methods for electron affinities of closed-shell molecules. *J. Chem. Phys.* **2020**, *152*, 124111.
- (128) Boguslawski, K. Open-shell extensions to closed-shell pCCD. *Chem. Commun.* **2021**, *57*, 12277–12280.
- (129) Gałyńska, M.; Tecmer, P.; Boguslawski, K. Exploring Electron Affinities, LUMO Energies, and Band Gaps with Electron-Pair Theories. *J. Phys. Chem. A* **2024**, *128*, 11068–11073.
- (130) Gałyńska, M.; Boguslawski, K. Benchmarking Ionization Potentials from pCCD Tailored Coupled Cluster Models. *J. Chem. Theory Comput.* **2024**, *20*, 4182–4195.
- (131) Behjou, S.; Tecmer, P.; Boguslawski, K. Electron Affinities from Equation-of-Motion Frozen Pair-Type Coupled Cluster Methods and Their Dependence on Single Excitations, Molecular Orbitals, and Basis Set Sizes. *J. Chem. Theory Comput.* **2025**, *21*, 10315–10328.
- (132) Thomas, S.; Hampe, F.; Stopkowicz, S.; Gauss, J. Complex ground-state and excitation energies in coupled-cluster theory. *Mol. Phys.* **2021**, *119*, e1968056.

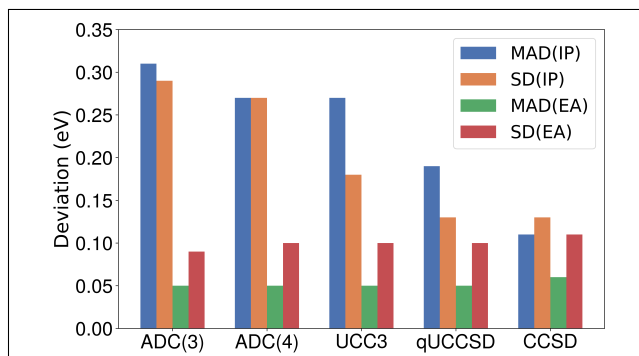
- (133) Hättig, C. Structure Optimizations for Excited States with Correlated Second-Order Methods: CC2 and ADC(2). *Adv. Quant. Chem.* **2005**, *50*, 37–60.
- (134) Köhn, A.; Tajti, A. Can coupled-cluster theory treat conical intersections? *J. Chem. Phys.* **2007**, *127*, 044105.
- (135) Kjøenstad, E. F.; Myhre, R. H.; Martínez, T. J.; Koch, H. Crossing conditions in coupled cluster theory. *J. Chem. Phys.* **2017**, *147*, 164105.
- (136) Kjøenstad, E. F.; Koch, H. Resolving the Notorious Case of Conical Intersections for Coupled Cluster Dynamics. *J. Phys. Chem. Lett.* **2017**, *8*, 4801–4807.
- (137) Kjøenstad, E. F.; Koch, H. An Orbital Invariant Similarity Constrained Coupled Cluster Model. *J. Chem. Theory Comput.* **2019**, *15*, 5386–5397.
- (138) Kjøenstad, E. F.; Angelico, S.; Koch, H. Coupled Cluster Theory for Nonadiabatic Dynamics: Nuclear Gradients and Nonadiabatic Couplings in Similarity Constrained Coupled Cluster Theory. *J. Chem. Theory Comput.* **2024**, 7080–7092.
- (139) Kutzelnigg, W. Quantum chemistry in Fock space. I. The universal wave and energy operators. *J. Chem. Phys.* **1982**, *77*, 3081–3097.
- (140) Hoffmann, M. R.; Simons, J. A unitary multiconfigurational coupled-cluster method: Theory and applications. *J. Chem. Phys.* **1988**, *88*, 993–1002.
- (141) Bartlett, R. J.; Kucharski, S. A.; Noga, J. Alternative coupled-cluster ansätze II. The unitary coupled-cluster method. *Chem. Phys. Lett.* **1989**, *155*, 133–140.
- (142) Watts, J. D.; Trucks, G. W.; Bartlett, R. J. The Unitary Coupled-Cluster Approach and Molecular Properties. Application of The UCC(4) Method. *Chem. Phys. Lett.* **1989**, *157*, 359–366.
- (143) Kutzelnigg, W. Error analysis and improvements of coupled-cluster theory. *Theor. Chim. Acta.* **1991**, *80*, 349–386.

- (144) Taube, A. G.; Bartlett, R. J. New perspectives on unitary coupled-cluster theory. *Int. J. Quantum Chem.* **2006**, *106*, 3393–3401.
- (145) Cooper, B.; Knowles, P. J. Benchmark studies of variational, unitary and extended coupled cluster methods. *J. Chem. Phys.* **2010**, *133*, 234102.
- (146) Evangelista, F. A. Alternative single-reference coupled cluster approaches for multireference problems: The simpler, the better. *J. Chem. Phys.* **2011**, *134*, 224102.
- (147) Wälz, G.; Kats, D.; Usvyat, D.; Korona, T.; Schütz, M. Application of Hermitian time-dependent coupled-cluster response Ansätze of second order to excitation energies and frequency-dependent dipole polarizabilities. *Phys. Rev. A* **2012**, *86*, 052519.
- (148) Harsha, G.; Shiozaki, T.; Scuseria, G. E. On the difference between variational and unitary coupled cluster theories. *J. Chem. Phys.* **2018**, *148*, 044107.
- (149) Phillips, J. T.; Koulias, L. N.; Yuwono, S. H.; DePrince III, A. E. Comparing perturbative and commutator-rank-based truncation schemes in unitary coupled-cluster theory. *Mol. Phys.* **2025**, e2522382.
- (150) Weiner, B.; Goscinski, O. Self-Consistent Approximation to the Polarization Propagator. *Int. J. Quant. Chem.* **1980**, *18*, 1109–1131.
- (151) Prasad, M. D.; Pal, S.; Mukherjee, D. Some aspects of self-consistent propagator theories. *Phys. Rev. A* **1985**, *31*, 1287–1298.
- (152) Datta, B. D.; Mukhopadhyay, D.; Mukherjee, D. Consistent propagator theory based on the extended coupled-cluster parametrization of the ground state. *Phys. Rev. A* **1993**, *47*, 3632–3648.
- (153) Hodecker, M.; Rehn, D. R.; Dreuw, A. Hermitian second-order methods for excited electronic states: Unitary coupled cluster in comparison with algebraic–diagrammatic construction schemes. *J. Chem. Phys.* **2020**, *152*, 094106.

- (154) Dempwolff, A. L.; Hodecker, M.; Dreuw, A. Vertical ionization potential benchmark for unitary coupled-cluster and algebraic-diagrammatic construction methods. *J. Chem. Phys.* **2022**, *156*, 054114.
- (155) Hodecker, M.; Dempwolff, A. L.; Schirmer, J.; Dreuw, A. Theoretical analysis and comparison of unitary coupled-cluster and algebraic-diagrammatic construction methods for ionization. *J. Chem. Phys.* **2022**, *156*, 074104.
- (156) Hodecker, M.; Dreuw, A.; Dempwolff, A. L. Unitary coupled-cluster theory for the electron propagator: electron attachment and physical properties *via* the intermediate state representation. *Phys. Chem. Chem. Phys.* **2025**, *27*, 16418–16427.
- (157) Sangfelt, E.; Kurtz, H. A.; Elander, N.; Goscinski, O. Excited states via the AGP polarization propagator. I. Application to Li_2 . *J. Chem. Phys.* **1984**, *81*, 3976–3986.
- (158) Löwdin, P.-O. Some properties of inner projections. *Int. J. Quantum Chem.* **1970**, *5*, 231–237.
- (159) Sun, Q. et al. Recent developments in the PySCF program package. *J. Chem. Phys.* **2020**, *153*, 024109.
- (160) Liu, J.; Shen, Y.; Asthana, A.; Cheng, L. Two-component relativistic coupled-cluster methods using mean-field spin-orbit integrals. *J. Chem. Phys.* **2018**, *148*, 034106.
- (161) Matthews, D. A.; Cheng, L.; Harding, M. E.; Lipparini, F.; Stopkowicz, S.; Jagau, T.-C.; Szalay, P. G.; Gauss, J.; Stanton, J. F. Coupled-cluster techniques for computational chemistry: The CFOUR program package. *J. Chem. Phys.* **2020**, *152*, 214108.
- (162) Stanton, J. F.; Gauss, J.; Cheng, L.; Harding, M. E.; Matthews, D. A.; Szalay, P. G. CFOUR, Coupled-Cluster techniques for Computational Chemistry, a quantum-chemical program package. <http://www.cfour.de>.

- (163) Ranasinghe, D. S.; Margraf, J. T.; Perera, A.; Bartlett, R. J. Vertical valence ionization potential benchmarks from equation-of-motion coupled cluster theory and QTP functionals. *J. Chem. Phys.* **2019**, *150*, 074108.

TOC Graphic



Supplementary Material for: Unitary
Coupled-Cluster based Self-Consistent
Electron Propagator Theory for
Electron-Detached and Electron-Attached
States: A Quadratic Unitary Coupled-Cluster
Singles and Doubles Method and Benchmark
Calculations

Yu Zhang and Junzi Liu*

*School of Chemistry and Biological Engineering, University of Science and Technology
Beijing, 100083 Beijing, China*

E-mail: jliu413@ustb.edu.cn

Table S1: Molecular geometries and basis sets used in vertical ionization potential (VIP) calculations with FCI reference values. All information is taken from ref. 1.

Molecule	Geometry	Basis set
H ₂ O	$R_{\text{OH}} = 0.957 \text{ \AA}$, $\angle\text{HOH} = 104.5^\circ$	6-31++G*
NH ₃	$R_{\text{NH}} = 1.0124 \text{ \AA}$, $\angle\text{HNH} = 106.67^\circ$	6-31++G*
HF	$R_{\text{HF}} = 0.917 \text{ \AA}$	6-31++G*
LiH	$R_{\text{LiH}} = 1.5957 \text{ \AA}$	aug-cc-pVDZ ^a
CO	$R_{\text{CO}} = 2.132 a_0$	cc-pVDZ
HCN	$R_{\text{HC}} = 1.064 \text{ \AA}$, $R_{\text{CN}} = 1.156 \text{ \AA}$	cc-pVDZ
NH ₂ ⁻	$R_{\text{NH}} = 1.0245 \text{ \AA}$, $\angle\text{NHN} = 103.34^\circ$	aug-cc-pVDZ ^b
CN ⁻	$R_{\text{CN}} = 1.1718 \text{ \AA}$	6-31+G
OH ⁻	$R_{\text{OH}} = 0.96966 \text{ \AA}$	cc-pVDZ
NO ₂ ⁻	$R_{\text{NO}} = 1.1934 \text{ \AA}$, $\angle\text{ONO} = 134.1^\circ$	6-31G
NO ₂ [•]	$R_{\text{NO}} = 1.1934 \text{ \AA}$, $\angle\text{ONO} = 134.1^\circ$	6-31G
NH ₂ [•]	$R_{\text{NH}} = 1.0245 \text{ \AA}$, $\angle\text{NHN} = 103.34^\circ$	aug-cc-pVDZ ^b
H ₂ O ^{•-}	$R_{\text{OH}} = 0.957 \text{ \AA}$, $\angle\text{HOH} = 104.5^\circ$	6-31++G*
NH ₃ ^{•-}	$R_{\text{NH}} = 1.0124 \text{ \AA}$, $\angle\text{HNH} = 106.67^\circ$	6-31++G*
HF ^{•-}	$R_{\text{HF}} = 0.917 \text{ \AA}$	6-31++G*
LiH ^{•-}	$R_{\text{LiH}} = 1.5957 \text{ \AA}$	aug-cc-pVDZ ^a

^a For Li, an earlier parametrization of polarization and diffuse functions [0.00864 (s), 0.00579 (p), 0.1239 (d), 0.0725 (d)] was employed.

^b A modified aug-cc-pVDZ basis without polarization diffuse functions was used on N and H atoms.

Table S2: 25 one-hole (1h)-dominated vertical ionization potentials (eV) for neutral singlet molecules and anions with closed-shell reference, computed using FCI, EOM-IP-CCSD, IP-ADC(3), IP-ADC(4), IP-UCC3, and IP-qUCCSD. To avoid redundancy, the names of the approximate methods are simplified to CCSD, ADC(3), ADC(4), UCC3, qUCCSD in the table header. Target states correspond to $(N - 1)$ -electron configurations relative to the RHF reference. For CO, HCN, and NO_2^- , CISDTQ results are listed in the ‘‘FCI’’ column. FCI and IP-ADC(3) data are from ref. 1; IP-ADC(4) data are from ref. 2.

Molecule/target states	config.	FCI	CCSD	ADC(3)	ADC(4)	UCC3	qUCCSD
LiH	$^1\Sigma^+$						
$1^2\Sigma^+$	$2\sigma^{-1}$	7.94	7.94	7.81	7.90	7.89	7.85
NH_3	1A_1						
1^2A	$3a^{-1}$	10.46	10.44	10.57	10.36	10.63	10.60
1^2E	$1e^{-1}$	16.40	16.39	16.50	16.28	16.62	16.54
H_2O	1A_1						
1^2B_1	$1b_1^{-1}$	12.30	12.17	12.72	11.98	12.57	12.52
1^2A_1	$3a_1^{-1}$	14.63	14.50	15.04	14.29	14.93	14.84
1^2B_2	$1b_2^{-1}$	18.97	18.89	19.30	18.67	19.25	19.13
HF	$^1\Sigma^+$						
$1^2\Pi$	$1\pi^{-1}$	15.93	15.69	16.68	15.35	16.31	16.21
$1^2\Sigma^+$	$3\sigma^{-1}$	19.98	19.78	20.58	19.49	20.30	20.16
CO	$^1\Sigma^+$						
$1^2\Sigma^+$	$5\sigma^{-1}$	13.56	13.83	13.38	13.62	13.65	13.62
$1^2\Pi$	$1\pi^{-1}$	16.68	16.75	16.88	16.57	16.68	16.63
$2^2\Sigma^+$	$4\sigma^{-1}$	19.39	19.49	20.23	18.59	19.88	19.68
HCN	$^1\Sigma^+$						
$1^2\Pi$	$1\pi^{-1}$	13.45	13.66	13.26	13.53	13.46	13.44
$1^2\Sigma^+$	$5\sigma^{-1}$	13.59	13.63	13.90	13.44	13.89	13.86

(continued)

Table S2 – (continued)

Molecule/target states	config.	FCI	CCSD	ADC(3)	ADC(4)	UCC3	qUCCSD
$2^2\Sigma^+$	$4\sigma^{-1}$	20.14	20.37	20.22	20.15	20.30	20.28
NH_2^-	1A_1						
1^2B_1	$1b_1^{-1}$	0.31	0.35	0.70	-0.18	0.55	0.43
1^2A_1	$3a_1^{-1}$	2.49	2.55	3.09	1.75	3.04	2.81
2^2B_2	$1b_2^{-1}$	7.02	7.13	7.63	6.18	7.63	7.36
OH^-	$^1\Sigma^+$						
$1^2\Pi$	$1\pi^{-1}$	-0.62	-0.73	-0.47	-0.68	-0.43	-0.45
$1^2\Sigma^+$	$3\sigma^{-1}$	3.74	3.68	3.80	3.71	3.85	3.83
CN^-	$^1\Sigma^+$						
$1^2\Sigma^+$	$5\sigma^{-1}$	3.26	3.41	3.22	3.23	3.48	3.46
$1^2\Pi$	$1\pi^{-1}$	5.11	5.29	5.02	4.96	5.42	5.23
$2^2\Sigma^+$	$4\sigma^{-1}$	6.46	6.60	7.01	6.12	7.01	6.92
NO_2^-	1A_1						
1^2A_1	$6a_1^{-1}$	-0.17	-0.08	-0.08	-0.17	0.14	0.11
1^2B_2	$4b_2^{-1}$	3.32	3.41	3.91	2.90	3.90	3.74
1^2A_2	$1a_2^{-1}$	3.58	3.59	3.61	3.67	3.65	3.62

Table S3: 17 one-hole (1h)-dominated vertical ionization potentials (eV) for radical, neutral triplet molecules, and radical anions with open-shell reference, computed using FCI, EOM-IP-CCSD, IP-ADC(3), IP-ADC(4), IP-UCC3, and IP-qUCCSD methods. To avoid redundancy, the names of the approximate methods are simplified to CCSD, ADC(3), ADC(4), UCC3, qUCCSD in the table header. Target states correspond to $(N - 1)$ -electron configurations relative to the UHF reference. For NO_2^\bullet and $\text{HCN}^{\bullet-}$, CISDTQ results are shown in the ‘‘FCI’’ column. FCI and IP-ADC(3) data are from ref. 1; IP-ADC(4) data are from ref. 2.

Molecule/target states	config.	FCI	CCSD	ADC(3)	ADC(4)	UCC3	qUCCSD
NH_2^\bullet	${}^2\text{B}_1$						
${}^3\text{B}_1$	$3a_1^{-1}$	11.68	11.63	11.75	11.57	11.81	11.75
${}^1\text{A}_1$	$1b_1^{-1}$	12.20	12.21	12.34	12.11	12.35	12.35
NO_2^\bullet	${}^2\text{A}_1$						
${}^1\text{A}_1$	$6a_1^{-1}$	10.84	10.80	10.78	10.35	11.10	11.06
${}^3\text{B}_2$	$4b_2^{-1}$	13.19	12.56	12.56	12.66	12.65	12.61
NH_3^*	${}^3\text{A}(3a \rightarrow 4a)$						
${}^2\text{A}$	$4a^{-1}$	4.46	4.45	4.43	4.44	4.46	4.43
${}^2\text{A}$	$3a^{-1}$	17.54	17.87	17.94	17.57	17.88	17.86
H_2O^*	${}^3\text{B}_1(1b_1 \rightarrow 4a_1)$						
${}^2\text{B}_1$	$4a_1^{-1}$	5.30	5.28	5.28	5.28	5.29	5.27
${}^4\text{B}_1$	$3a_1^{-1}$	18.68	18.90	19.02	18.52	18.91	18.84
${}^2\text{A}_1$	$1b_1^{-1}$	19.99	20.33	20.61	19.91	20.46	20.43
$\text{LiH}^{\bullet-}$	${}^2\Sigma^+$						
${}^1\Sigma^+$	$3\sigma^{-1}$	0.30	0.30	0.29	0.30	0.30	0.30
${}^3\Sigma^+$	$2\sigma^{-1}$	3.49	3.75	3.41	3.49	3.43	3.36
$\text{NH}_3^{\bullet-}$	${}^2\text{A}$						
${}^1\text{A}$	$4a^{-1}$	-0.95	-0.97	-0.98	-0.97	-0.96	-0.98
${}^3\text{A}$	$3a^{-1}$	5.04	5.28	5.35	4.87	5.38	5.27
$\text{H}_2\text{O}^{\bullet-}$	${}^2\text{A}_2$						

(continued)

Table S3 – (continued)

Molecule/target states	config.	FCI	CCSD	ADC(3)	ADC(4)	UCC3	qUCCSD
1^1A_1	$4a_1^{-1}$	-0.94	-0.95	-0.96	-0.96	-0.94	-0.96
1^3B_1	$1b_1^{-1}$	6.06	6.30	6.70	5.69	6.53	6.37
HF \bullet^-	$2\Sigma^+$						
$1^1\Sigma^+$	$4\sigma^{-1}$	-0.99	-1.01	-1.00	-1.01	-0.99	-1.01
$1^3\Pi$	$1\pi^{-1}$	9.00	9.25	9.91	8.37	9.58	9.37

Table S4: 201 1h-dominated vertical ionization potentials (eV) for neutral molecules with closed-shell reference states, computed using EOM-IP-CCSDTQ, EOM-IP-CCSDT, EOM-IP-CCSD, IP-ADC(3), IP-ADC(4), IP-UCC3, and IP-qUCCSD methods. To avoid redundancy, the names of the approximate methods are simplified to CCSD, ADC(3), ADC(4), UCC3, qUCCSD in the table header. Target states correspond to $(N - 1)$ -electron configurations relative to the RHF reference. The cc-pVTZ basis set was used for all calculations. Molecular geometries and IP-EOM-CCSDTQ/IP-EOM-CCSDT results are from ref. 3; IP-ADC(3) and IP-ADC(4) results are from ref. 2.

Molecule	config.	CCSDTQ	CCSDT	CCSD	ADC(3)	ADC(4)	UCC3	qUCCSD
CO	$5\sigma^{-1}$	13.88	13.90	14.14	13.69	13.93	13.94	13.92
	$1\pi^{-1}$	16.94	16.95	17.01	17.06	16.82	16.89	16.84
	$4\sigma^{-1}$	19.57	19.54	19.74	20.34	18.79	20.03	19.84
H ₂ O	$1b_1^{-1}$	12.49	12.45	12.40	12.73	12.33	12.67	12.65
	$3a_1^{-1}$	14.73	14.69	14.63	14.94	14.57	14.90	14.86
	$1b_2^{-1}$	18.86	18.84	18.81	18.98	18.75	18.97	18.93
HF	$1\pi^{-1}$	15.95	15.90	15.81	16.39	15.66	16.23	16.17
	$3\sigma^{-1}$	19.86	19.83	19.75	20.15	19.65	20.02	19.97
F ₂	$1\pi_g^{-1}$	15.61	15.58	15.51	15.86	15.39	15.84	15.74
	$1\pi_u^{-1}$	18.73	18.74	18.82	19.04	18.45	18.96	18.84
	$3\sigma_g^{-1}$	20.96	20.96	21.05	20.86	20.92	20.98	20.91
HCl	$2\pi^{-1}$	12.59	12.58	12.63	12.58	12.56	12.56	12.57
	$5\sigma^{-1}$	16.58	16.57	16.64	16.58	16.56	16.56	16.57
	$4\sigma^{-1}$	26.49	26.63	25.69	26.82	26.54	26.85	26.84
CH ₄	$1t_2^{-1}$	14.36	14.35	14.38	14.32	14.34	14.40	14.40
	$2a_1^{-1}$	23.12	23.11	23.35	23.21	23.10	23.34	23.33
NH ₃	$3a_1^{-1}$	10.76	10.74	10.73	10.81	10.72	10.85	10.84
	$1e_1^{-1}$	16.50	16.48	16.48	16.51	16.45	16.59	16.56
N ₂	$3\sigma_g^{-1}$	15.42	15.45	15.57	15.44	15.47	15.53	15.57

(continued)

Table S4 – (continued)

Molecule	config.	CCSDTQ	CCSDT	CCSD	ADC(3)	ADC(4)	UCC3	qUCCSD
CO ₂	$1\pi_u^{-1}$	16.88	16.89	17.17	16.53	17.06	16.81	16.82
	$2\sigma_u^{-1}$	18.60	18.67	18.83	18.81	18.61	18.82	18.80
	$1\pi_g^{-1}$	13.64	13.63	13.70	13.74	13.50	13.72	13.62
	$1\pi_u^{-1}$	17.46	17.50	17.95	17.74	17.15	17.77	17.57
	$3\sigma_u^{-1}$	17.88	17.84	18.09	18.51	17.26	18.43	18.23
	$4\sigma_g^{-1}$	19.11	19.08	19.41	19.90	18.34	19.78	19.54
C ₂ H ₂	$1\pi_u^{-1}$	11.42	11.42	11.54	11.19	11.47	11.33	11.34
	$3\sigma_g^{-1}$	17.10	17.12	17.24	17.18	17.08	17.22	17.26
	$2\sigma_u^{-1}$	18.97	19.00	19.15	19.15	18.92	19.18	19.14
	$2\sigma_g^{-1}$	23.60	23.70	24.43	23.80	23.77	23.86	23.87
HCN	$1\pi^{-1}$	13.71	13.72	13.89	13.44	13.79	13.63	13.63
	$5\sigma^{-1}$	13.83	13.84	13.92	14.12	13.68	14.08	14.08
	$4\sigma^{-1}$	20.36	20.43	20.63	20.44	20.38	20.51	20.50
H ₂ CO	$2b_2^{-1}$	10.79	10.75	10.76	11.09	10.43	11.04	10.93
	$1b_1^{-1}$	14.50	14.50	14.55	14.40	14.36	14.38	14.33
	$5a_1^{-1}$	16.01	15.96	16.03	16.47	15.49	16.43	16.25
	$1b_2^{-1}$	17.05	17.10	17.44	17.15	16.90	17.20	17.14
	$4a_1^{-1}$	21.24	21.30	21.72	21.44	21.08	21.53	21.45
P ₂	$2\pi_u^{-1}$	10.49	10.51	10.56	10.29	10.54	10.25	10.28
	$5\sigma_g^{-1}$	10.64	10.65	10.74	10.62	10.60	10.56	10.59
CS	$7\sigma^{-1}$	11.23	11.26	11.47	11.02	11.34	11.26	11.27
	$2\pi^{-1}$	12.85	12.88	12.96	12.63	13.01	12.63	12.64
	$6\sigma^{-1}$	17.89	18.08	17.17	17.98	17.90	17.88	17.77
OCS	$3\pi^{-1}$	-	11.12	11.20	10.93	11.18	10.99	10.97

(continued)

Table S4 – (continued)

Molecule	config.	CCSDTQ	CCSDT	CCSD	ADC(3)	ADC(4)	UCC3	qUCCSD
	$2\pi^{-1}$	-	15.61	16.14	15.76	15.24	15.73	15.47
	$9\sigma^{-1}$	-	15.83	16.10	15.90	15.63	15.98	15.93
	$8\sigma^{-1}$	-	17.89	18.40	18.90	17.01	18.68	18.36
FCN	$2\pi^{-1}$	-	13.50	13.70	13.26	13.58	13.48	13.45
	$7\sigma^{-1}$	-	14.31	14.44	14.54	14.17	14.56	14.54
	$1\pi^{-1}$	-	19.39	19.67	20.10	18.89	19.91	19.76
	$6\sigma^{-1}$	-	22.79	23.07	23.36	22.32	23.27	23.10
C_2H_6	$1e_g^{-1}$	-	12.68	12.71	12.66	12.66	12.73	12.72
	$3a_{1g}^{-1}$	-	13.06	13.11	13.08	13.03	13.16	13.18
	$1e_u^{-1}$	-	15.38	15.44	15.40	15.35	15.48	15.47
	$2b_u^{-1}$	-	20.69	20.90	20.82	20.66	20.91	20.89
	$2a_{1g}^{-1}$	-	24.15	24.60	24.45	24.08	24.56	24.54
CH_2F_2	$2b_1^{-1}$	-	13.29	13.35	13.54	13.08	13.54	13.47
	$4b_2^{-1}$	-	14.92	14.95	15.56	14.53	15.37	15.25
	$6a_1^{-1}$	-	15.20	15.25	15.61	14.91	15.51	15.43
	$1a_2^{-1}$	-	15.59	15.66	16.32	15.15	16.13	15.99
	$3b_2^{-1}$	-	18.75	18.85	19.19	18.45	19.10	18.98
	$5a_1^{-1}$	-	18.97	19.13	19.39	18.70	19.34	19.24
	$1b_1^{-1}$	-	19.15	19.33	19.51	18.93	19.51	19.42
CH_3F	$2e_1^{-1}$	-	13.17	13.18	13.48	12.92	13.43	13.37
	$5a_1^{-1}$	-	17.01	17.04	17.29	16.78	17.21	17.15
	$1e_1^{-1}$	-	17.04	17.14	17.42	16.84	17.36	17.29
	$4a_1^{-1}$	-	23.51	23.79	23.69	23.41	23.78	23.72
CHF_3	$6a_1^{-1}$	-	14.76	14.87	15.02	14.58	15.02	14.95

(continued)

Table S4 – (continued)

Molecule	config.	CCSDTQ	CCSDT	CCSD	ADC(3)	ADC(4)	UCC3	qUCCSD
CH ₃ CCH	$1a_2^{-1}$	-	15.33	15.40	15.96	14.98	15.80	15.68
	$5e_1^{-1}$	-	15.93	16.02	16.52	15.58	16.39	16.26
	$4e_1^{-1}$	-	16.99	17.11	17.59	16.64	17.46	17.33
	$3e_1^{-1}$	-	20.41	20.59	20.87	20.11	20.83	20.69
	$5a_1^{-1}$	-	20.93	21.81	21.31	20.69	21.34	21.23
	$4a_1^{-1}$	-	24.43	24.74	24.86	24.16	24.88	24.75
	$2e_1^{-1}$	-	10.46	10.57	10.24	10.50	10.39	10.38
	$1e_1^{-1}$	-	15.17	15.28	15.21	15.13	15.27	15.26
	$7a_1^{-1}$	-	15.22	15.35	15.31	15.17	15.39	15.41
NSF	$6a_1^{-1}$	-	17.65	17.83	17.81	17.54	17.85	17.81
	$13a'^{-1}$	-	11.62	11.76	11.45	11.54	11.21	11.55
	$12a'^{-1}$	-	13.30	13.52	13.47	12.91	13.51	13.43
	$3a''^{-1}$	-	13.74	13.92	13.67	13.32	13.79	13.71
	$11a'^{-1}$	-	15.24	15.59	16.34	14.36	16.09	15.97
	$2a''^{-1}$	-	16.11	16.48	17.03	15.52	16.48	16.36
HCOOH	$10a'^{-1}$	-	16.35	16.86	17.25	15.71	17.14	16.75
	$10a'^{-1}$	-	11.33	11.40	11.74	10.97	11.68	11.53
	$2a''^{-1}$	-	12.47	12.52	12.60	12.34	12.56	12.47
	$9a'^{-1}$	-	14.79	14.92	15.19	14.47	15.20	15.05
	$1a''^{-1}$	-	15.71	16.02	15.93	15.48	15.95	15.78
	$8a'^{-1}$	-	17.06	17.32	17.78	16.49	17.71	17.48
	$7a'^{-1}$	-	17.81	18.18	18.07	17.56	18.15	18.03
	$6a'^{-1}$	-	22.08	22.57	22.59	21.84	22.67	22.55
SiO	$7\sigma^{-1}$	-	11.33	11.43	11.70	10.09	11.66	11.47

(continued)

Table S4 – (continued)

Molecule	config.	CCSDTQ	CCSDT	CCSD	ADC(3)	ADC(4)	UCC3	qUCCSD	
H ₂ CS	$2\pi^{-1}$	-	11.87	11.92	12.64	10.74	12.13	11.88	
	$6\sigma^{-1}$	-	14.58	15.05	15.51	13.43	15.21	14.86	
	$3b_2^{-1}$	-	9.25	9.27	9.22	9.16	9.29	9.19	
	$2b_1^{-1}$	-	11.78	11.83	11.52	11.78	11.61	11.59	
	$7a_1^{-1}$	-	13.88	13.99	13.85	13.86	13.88	13.88	
	$2b_2^{-1}$	-	15.61	15.98	15.60	15.41	15.61	15.61	
CF ₄	$6a_1^{-1}$	-	19.60	19.50	19.57	19.36	19.58	19.53	
	$1t_1^{-1}$	-	16.09	16.21	16.66	15.79	16.55	16.43	
	$4t_2^{-1}$	-	17.24	17.37	17.68	16.98	17.63	17.51	
	$1e^{-1}$	-	18.18	18.36	18.76	17.87	18.67	18.55	
	$3t_2^{-1}$	-	21.93	22.18	22.37	21.67	22.37	22.24	
	$4a_1^{-1}$	-	24.85	25.16	25.39	24.54	25.38	25.23	
SiF ₄	$1t_1^{-1}$	-	16.23	16.37	16.90	15.85	16.72	16.58	
	$5t_2^{-1}$	-	17.24	17.40	17.88	16.86	17.72	17.58	
	$1e^{-1}$	-	17.63	17.80	18.28	17.23	18.12	17.99	
	$4t_2^{-1}$	-	19.17	19.35	19.80	18.76	19.66	19.52	
	$5a_1^{-1}$	-	21.27	21.49	21.94	20.83	21.80	21.66	
	$2\pi^{-1}$	-	11.34	11.49	11.13	11.39	11.30	11.29	
HCCF	$1\pi^{-1}$	-	17.90	18.12	18.73	17.33	18.47	18.32	
	$7\sigma^{-1}$	-	18.12	18.29	18.19	18.07	18.28	18.27	
	$6\sigma^{-1}$	-	20.95	21.26	21.71	20.50	21.59	21.47	
	$5\sigma^{-1}$	-	24.40	25.29	24.51	24.39	24.60	24.59	
	NNO	$2\pi^{-1}$	-	12.74	12.83	12.63	12.53	12.73	12.65
		$7\sigma^{-1}$	-	16.28	16.64	16.28	16.25	16.60	16.51

(continued)

Table S4 – (continued)

Molecule	config.	CCSDTQ	CCSDT	CCSD	ADC(3)	ADC(4)	UCC3	qUCCSD
CH ₃ NC	1 π^{-1}	-	18.31	19.00	19.05	17.87	19.14	19.07
	6 σ^{-1}	-	19.89	20.15	20.94	18.45	20.61	20.26
	7 a_1^{-1}	-	11.21	11.45	11.04	11.21	11.24	11.22
	2 e_1^{-1}	-	12.55	12.64	12.50	12.53	12.51	12.48
	1 e_1^{-1}	-	16.59	16.68	16.81	16.41	16.74	16.68
	6 a_1^{-1}	-	18.38	18.61	18.40	18.08	18.35	18.33
CH ₃ CN	5 a_1^{-1}	-	25.06	25.48	25.68	24.79	25.64	25.62
	2 e_1^{-1}	-	12.45	12.60	12.19	12.51	12.38	12.35
	7 a_1^{-1}	-	12.97	13.11	13.28	12.77	13.27	13.23
	1 e_1^{-1}	-	16.24	16.40	16.22	16.23	16.32	16.31
	6 a_1^{-1}	-	17.38	17.54	17.42	17.34	17.53	17.54
	5 a_1^{-1}	-	24.88	25.36	25.30	24.79	25.40	25.39
gem-C ₂ H ₂ F ₂	2 b_1^{-1}	-	10.54	10.64	10.39	10.54	10.55	10.51
	5 b_2^{-1}	-	14.96	15.10	15.17	14.64	15.23	15.17
	8 a_1^{-1}	-	15.52	15.69	15.81	15.26	15.82	15.76
	4 b_2^{-1}	-	15.85	16.01	16.37	15.62	16.23	16.10
	1 a_2^{-1}	-	16.02	16.22	16.74	15.58	16.52	16.39
	7 a_1^{-1}	-	18.27	18.35	18.51	17.85	18.48	18.39
	1 b_1^{-1}	-	18.10	18.39	18.76	17.99	18.62	18.48
	3 b_2^{-1}	-	19.63	19.89	20.14	19.24	20.05	19.90
	6 a_1^{-1}	-	21.41	21.81	22.04	21.00	22.00	21.70
	5 a_1^{-1}	-	25.10	25.58	25.36	25.12	25.43	25.41
cis-C ₂ H ₂ F ₂	2 b_1^{-1}	-	10.39	10.47	10.27	10.34	10.41	10.37
	7 a_1^{-1}	-	13.88	14.01	14.24	13.55	14.20	14.13

(continued)

Table S4 – (continued)

Molecule	config.	CCSDTQ	CCSDT	CCSD	ADC(3)	ADC(4)	UCC3	qUCCSD	
O ₃	$6b_2^{-1}$	-	14.80	14.94	15.32	14.32	15.22	15.10	
	$1a_2^{-1}$	-	16.07	16.22	16.84	15.53	16.57	16.44	
	$5b_2^{-1}$	-	16.85	17.08	17.40	16.67	17.31	17.20	
	$1b_1^{-1}$	-	16.97	17.11	17.52	16.38	17.35	17.20	
	$6a_1^{-1}$	-	18.50	18.71	18.97	18.11	18.90	18.79	
	$5a_1^{-1}$	-	18.88	19.17	19.24	18.55	19.24	19.15	
	$4b_2^{-1}$	-	20.85	21.19	21.30	20.47	21.26	21.13	
	$4a_2^{-1}$	-	24.61	25.09	24.70	24.62	24.77	24.72	
	$6a_1^{-1}$	-	12.54	12.74	12.72	11.99	12.93	12.67	
	$4b_2^{-1}$	-	12.69	12.87	12.87	12.02	12.93	12.69	
	$1a_2^{-1}$	-	13.46	13.43	12.63	13.58	12.63	12.83	
	$1b_1^{-1}$	-	21.32	18.80	20.76	21.20	21.30	20.97	
	HCONH ₂	$10a'^{-1}$	-	10.17	10.29	10.60	9.71	10.58	10.40
		$2a''^{-1}$	-	10.56	10.61	10.68	10.48	10.59	10.52
$1a''^{-1}$		-	14.06	14.44	14.17	13.86	14.20	14.00	
$9a'^{-1}$		-	14.67	14.88	15.28	14.09	15.23	15.00	
$8a'^{-1}$		-	16.55	16.90	16.93	16.32	17.00	16.90	
$7a'^{-1}$		-	19.25	19.06	19.29	18.99	19.36	19.36	
$6a'^{-1}$		-	20.90	21.26	21.11	20.68	21.20	21.13	
C ₂ H ₄	$1b_{3u}^{-1}$	-	10.64	10.66	10.44	10.62	10.59	10.55	
	$1b_{3g}^{-1}$	-	13.08	13.12	13.05	13.04	13.11	13.11	
	$3a_g^{-1}$	-	14.79	14.90	14.80	14.77	14.87	14.90	
	$1b_{2u}^{-1}$	-	16.14	16.31	16.11	16.05	16.20	16.17	
	$2b_{1u}^{-1}$	-	19.32	19.60	19.31	19.22	19.40	19.35	

(continued)

Table S4 – (continued)

Molecule	config.	CCSDTQ	CCSDT	CCSD	ADC(3)	ADC(4)	UCC3	qUCCSD
C ₂ F ₄	2a _g ⁻¹	-	23.87	24.43	24.06	23.77	24.11	24.11
	2b _{3u} ⁻¹	-	10.37	10.51	10.22	10.37	10.43	10.39
	4b _{3g} ⁻¹	-	15.78	15.97	16.50	15.30	16.32	16.18
	6a _g ⁻¹	-	16.11	16.31	16.52	15.79	16.49	16.40
	4b _{2u} ⁻¹	-	16.32	16.53	17.00	15.82	16.84	16.70
	1a _u ⁻¹	-	16.48	16.70	17.17	16.02	17.00	16.86
	1b _{1g} ⁻¹	-	16.64	16.88	17.34	16.17	17.17	17.03
	5b _{1u} ⁻¹	-	17.32	17.56	18.03	16.83	17.86	17.73
	1b _{2g} ⁻¹	-	18.02	18.26	18.65	17.63	18.52	18.39
	1b _{3u} ⁻¹	-	19.12	19.50	19.67	18.73	19.64	19.48
	3b _{3g} ⁻¹	-	19.41	19.64	19.87	19.06	19.83	19.67
	3b _{2u} ⁻¹	-	20.76	20.99	21.17	20.30	21.14	20.99
HCCCN	5a _g ⁻¹	-	21.03	21.32	21.50	20.60	21.49	21.36
	2π ⁻¹	-	11.69	11.87	11.41	11.74	11.57	11.55
	9σ ⁻¹	-	13.44	13.69	13.88	13.09	13.82	13.71
	1π ⁻¹	-	14.19	14.48	13.91	14.15	14.04	13.94
	8σ ⁻¹	-	18.53	18.81	18.69	18.39	18.73	18.72
	7σ ⁻¹	-	21.55	21.95	21.91	21.35	21.94	21.94
	6σ ⁻¹	-	25.31	25.89	25.49	25.23	25.51	25.50
C ₂ N ₂	1π _g ⁻¹	-	13.48	13.71	13.15	13.55	13.36	13.32
	5σ _g ⁻¹	-	14.40	14.66	14.76	14.12	14.72	14.66
	4σ _u ⁻¹	-	14.77	15.04	15.16	14.45	15.10	15.03
	1π _u ⁻¹	-	15.70	16.05	15.37	15.70	15.54	15.44
	4σ _g ⁻¹	-	23.29	23.93	23.44	23.21	23.53	23.55

(continued)

Table S4 – (continued)

Molecule	config.	CCSDTQ	CCSDT	CCSD	ADC(3)	ADC(4)	UCC3	qUCCSD
C ₃ O ₂	2 π_u^{-1}	-	10.62	10.70	10.32	10.73	10.46	10.43
	1 π_g^{-1}	-	14.92	15.58	15.04	14.21	14.95	14.73
	1 π_u^{-1}	-	15.72	16.33	16.08	15.20	16.02	15.72
	5 σ_u^{-1}	-	17.10	17.66	18.28	15.80	18.01	17.63
	6 σ_g^{-1}	-	17.28	17.87	18.57	15.91	18.23	17.83
	4 σ_u^{-1}	-	22.22	22.91	22.82	22.38	22.99	22.95
	5 σ_g^{-1}	-	25.88	25.71	26.33	25.36	26.73	26.71
HC ₄ H	1 π_g^{-1}	-	10.20	10.34	9.96	10.23	10.09	10.07
	1 π_u^{-1}	-	12.70	12.94	12.50	12.63	12.60	12.52
	5 σ_g^{-1}	-	17.14	17.39	17.34	16.98	17.37	17.35
	4 σ_u^{-1}	-	17.82	18.10	18.03	17.64	18.05	17.99
	4 σ_g^{-1}	-	20.05	20.41	20.43	19.80	20.42	20.39
	3 σ_u^{-1}	-	23.42	24.05	23.82	23.23	23.84	23.81
	3 σ_g^{-1}	-	24.76	25.38	25.73	24.65	25.75	25.76

Table S5: Molecular geometry and basis sets used in vertical electron affinity (VEA) benchmark calculations with FCI reference values. All information is from ref. 4.

Molecule	Geometry	Basis set
H ₂ O	$R_{\text{OH}} = 0.957 \text{ \AA}$, $\angle\text{HOH} = 104.5^\circ$	O:6-31+G*, H:6-31++G
NH ₃	$R_{\text{NH}} = 1.0124 \text{ \AA}$, $\angle\text{HNH} = 106.67^\circ$	N:6-31+G*, H:6-31++G
HF	$R_{\text{HF}} = 0.917 \text{ \AA}$	F:6-31+G*, H:6-31++G
CO	$R_{\text{CO}} = 2.132 a_0$	cc-pVDZ
HCN	$R_{\text{HC}} = 1.064 \text{ \AA}$, $R_{\text{CN}} = 1.156 \text{ \AA}$	cc-pVDZ
LiH	$R_{\text{LiH}} = 1.5957 \text{ \AA}$	aug-cc-pVDZ ^a
CH ₂	$R_{\text{CH}} = 1.11656 \text{ \AA}$, $\angle\text{HCH} = 102.4^\circ$	cc-pVDZ ^b
NH ₂ ⁺	$R_{\text{NH}} = 1.0245 \text{ \AA}$, $\angle\text{HNH} = 103.34^\circ$	aug-cc-pVDZ ^c
BeH ⁺	$R_{\text{BeH}} = 1.3426 \text{ \AA}$	aug-cc-pVDZ
CH ⁺	$R_{\text{CH}} = 1.1309 \text{ \AA}$	aug-cc-pVDZ
CN ⁺	$R_{\text{CN}} = 1.1718 \text{ \AA}$	6-31+G
NO ₂ ⁺	$R_{\text{NO}} = 1.1934 \text{ \AA}$, $\angle\text{ONO} = 134.1^\circ$	6-31G
NO ₂ [•]	$R_{\text{NO}} = 1.1934 \text{ \AA}$, $\angle\text{ONO} = 134.1^\circ$	6-31G
NH ₂ [•]	$R_{\text{NH}} = 1.0245 \text{ \AA}$, $\angle\text{NHN} = 103.34^\circ$	aug-cc-pVDZ ^c
LiH ^{•+}	$R_{\text{LiH}} = 1.5957 \text{ \AA}$	aug-cc-pVDZ ^a
NH ₃ ^{•+}	$R_{\text{NH}} = 1.0124 \text{ \AA}$, $\angle\text{HNH} = 106.67^\circ$	6-31++G*
H ₂ O ^{•+}	$R_{\text{OH}} = 0.957 \text{ \AA}$, $\angle\text{HOH} = 104.5^\circ$	6-31++G*
CO ^{•+}	$R_{\text{CO}} = 2.132 a_0$	cc-pVDZ

^a For Li, an earlier parametrization of polarization and diffuse functions [0.00864 (s), 0.00579 (p), 0.1239 (d), 0.0725 (d)] was employed.

^b Here the cc-pVDZ basis is augmented with additional diffuse functions on C [0.015 (s)] and H [0.025 (s)] atoms.

^c A modified aug-cc-pVDZ basis without polarization diffuse functions was used on N and H atoms.

Table S6: 35 one-particle (1p)-dominated vertical electron affinities (eV) for neutral molecules and cations with closed-shell reference, computed using FCI, EOM-EA-CCSD, EA-ADC(3), EA-ADC(4), EA-UCC3, and EA-qUCCSD. To avoid redundancy, the names of the approximate methods are simplified to CCSD, ADC(3), ADC(4), UCC3, qUCCSD in the table header. Target states correspond to $(N + 1)$ -electron configurations relative to the RHF reference. For CO, HCN, and NO_2^+ , CISDTQ results are shown in the “FCI” column. FCI and IP-ADC(3) data are from ref. 4; EA-ADC(4) data are from ref. 2.

Molecule/target states	config.	FCI	CCSD	ADC(3)	ADC(4)	UCC3	qUCCSD
LiH	$^1\Sigma^+$						
$1^2\Sigma^+$	3σ	0.30	0.29	0.31	0.31	0.29	0.30
$1^2\Pi$	1π	-0.31	-0.32	-0.31	-0.31	-0.31	-0.31
$2^2\Sigma^+$	4σ	-0.49	-0.49	-0.48	-0.49	-0.49	-0.49
$3^2\Sigma^+$	5σ	-0.77	-0.78	-0.77	-0.77	-0.77	-0.79
$2^2\Pi$	2π	-1.20	-1.23	-1.22	-1.21	-1.22	-1.21
CH_2	1A_1						
1^2B_1	$1b_1$	0.16	0.08	0.28	0.30	0.23	0.22
1^2A_1	$4a_1$	-0.72	-0.74	-0.73	-0.73	-0.72	-0.72
1^2B_2	$2b_2$	-1.66	-1.65	-1.65	-1.65	-1.66	-1.66
2^2A_1	$5a_1$	-1.98	-1.98	-1.98	-1.98	-2.00	-2.00
NH_3	1A_1						
1^2A	$4a$	-0.95	-0.97	-0.96	-0.96	-0.97	-0.96
1^2E	$2e$	-1.94	-1.94	-1.94	-1.94	-1.94	-1.94
H_2O	1A_1						
1^2A_1	$4a_1$	-0.94	-0.96	-0.94	-0.94	-0.95	-0.95
1^2B_2	$2b_2$	-1.88	-1.89	-1.88	-1.88	-1.88	-1.88
2^2A_1	$5a_1$	-6.27	-6.31	-6.27	-6.28	-6.30	-6.28
1^2B_1	$2b_1$	-6.68	-6.76	-6.71	-6.61	-6.75	-6.72

(continued)

Table S6 – (continued)

Molecule/target states	config.	FCI	CCSD	ADC(3)	ADC(4)	UCC3	qUCCSD
2^2B_2	$3b_2$	-8.25	-8.30	-8.27	-8.27	-8.28	-8.28
HF	$1^1\Sigma^+$						
$1^2\Sigma^+$	4σ	-0.99	-1.01	-0.99	-1.00	-1.01	-1.00
$2^2\Sigma^+$	5σ	-7.34	-7.44	-7.31	-7.36	-7.40	-7.37
$3^2\Sigma^+$	6σ	-8.11	-8.18	-8.09	-8.14	-8.14	-8.13
$1^2\Pi$	2π	-8.30	-8.37	-8.28	-8.33	-8.34	-8.32
CO	$1^1\Sigma^+$						
$1^2\Pi$	2π	-3.62	-3.56	-3.53	-3.64	-3.56	-3.54
$1^2\Sigma^+$	6σ	-9.86	-9.79	-9.80	-9.77	-9.79	-9.79
HCN	$1^1\Sigma^+$						
$1^2\Sigma^+$	6σ	-4.41	-4.29	-4.48	-4.29	-4.48	-4.43
$1^2\Pi$	2π	-4.68	-4.33	-4.31	-4.37	-4.30	-4.30
$2^2\Sigma^+$	7σ	-8.90	-8.42	-8.53	-8.40	-8.49	-8.48
NH_2^+	1^1A_1						
1^2B_1	$1b_1$	12.20	12.24	12.21	12.34	12.08	12.08
2^2A_1	$4a_1$	4.67	4.67	4.69	4.69	4.65	4.65
2^2B_2	$2b_2$	3.00	3.02	3.01	3.01	2.99	2.99
CN^+	$1^1\Sigma^+$						
$1^2\Sigma^+$	5σ	13.08	13.43	14.70	14.08		14.16
$2^2\Pi$	2π	5.23	5.44	6.34	4.88	6.67	5.71
NO_2^+	1^1A_1						
1^2A_1	$6a_1$	10.84	10.92	11.24	10.50	11.33	11.22
1^2B_1	$2b_1$	8.02	8.30	8.60	7.73	8.77	8.70
BeH^+	$1^1\Sigma^+$						

(continued)

Table S6 – (continued)

Molecule/target states	config.	FCI	CCSD	ADC(3)	ADC(4)	UCC3	qUCCSD
$1^2\Sigma^+$	3σ	8.29	8.26	8.32	8.31	8.24	8.26
$2^2\Pi$	1π	5.77	5.72	5.77	5.77	5.75	5.76
$2^2\Sigma^+$	4σ	2.78	2.74	2.74	2.78	2.72	2.73
$2^2\Pi$	2π	1.87	1.87	1.87	1.93	1.87	1.87
$1^2\Delta$	1δ	0.01	-0.20	-0.02	0.01	-0.03	-0.03
CH ⁺	$1\Sigma^+$						
$1^2\Pi$	1π	10.42	10.41	10.57	10.52	10.41	10.39
$2^2\Sigma^+$	4σ	4.05	4.08	4.11	4.10	4.05	4.05

Table S7: 16 one-particle (1p)-dominated vertical electron affinities (eV) for radical, neutral triplet molecules and radical cations with open-shell reference, computed using FCI, EOM-EA-CCSD, EA-ADC(3), EA-ADC(4), EA-UCC3, and EA-qUCCSD. To avoid redundancy, the names of the approximate methods are simplified to CCSD, ADC(3), ADC(4), UCC3, qUCCSD in the table header. Target states correspond to $(N + 1)$ -electron configurations relative to the UHF reference. For NO_2^\bullet , CISDTQ results are shown in the ‘‘FCI’’ column. FCI and IP-ADC(3) data are from ref. 4; EA-ADC(4) data are from ref. 2.

Molecule/target states	config.	FCI	CCSD	ADC(3)	ADC(4)	UCC3	qUCCSD
NH_2^\bullet	2B_1						
1^1A_1	$1b_1$	0.31	0.22	-0.08	0.33	-0.09	0.01
1^3B_1	$4a_1$	-0.80	-0.81	-0.81	-0.80	-0.82	-0.81
2^3B_1	$5a_1$	-4.23	-4.26	-4.24	-4.23	-4.24	-4.23
NO_2^\bullet	2A_1						
1^1A_1	$6a_1$	-0.17	0.07	-0.01	-0.01	0.19	0.13
LiH^*	${}^3\Sigma^+(2\sigma \rightarrow 3\sigma)$						
$1^2\Sigma^+$	2σ	3.49	3.21	3.22	3.34	3.21	3.22
$1^4\Pi$	1π	-0.01	-0.02	-0.01	-0.01	-0.02	-0.02
NH_3^*	${}^3A(3a \rightarrow 4a)$						
1^2A	$3a$	5.04	4.88	4.51	5.13	4.41	4.51
H_2O^*	${}^3B_1(1b_1 \rightarrow 4a_1)$						
1^2A_1	$1b_1$	6.06	5.77	5.47	6.07	5.27	5.38
2^2B_1	$4a_1$	-0.15	-0.15	-0.08	-0.14	-0.13	-0.12
1^4A_2	$2b_2$	-0.77	-0.76	-0.73	-0.75	-0.77	-0.76
$\text{LiH}^{\bullet+}$	${}^2\Sigma^+$						
$1^1\Sigma^+$	2σ	7.94	7.93	7.94	7.94	7.94	7.94
$1^3\Sigma^+$	3σ	4.76	4.76	4.75	4.76	4.76	4.76
$\text{NH}_3^{\bullet+}$	2A						

(continued)

Table S7 – (continued)

Molecule/target states	config.	FCI	CCSD	ADC(3)	ADC(4)	UCC3	qUCCSD
1^1A	$3a$	10.46	10.52	10.14	10.48	10.14	10.18
1^3A	$4a$	4.46	4.45	4.46	4.46	4.45	4.45
$H_2O^{\bullet+}$	2B_1						
1^1A_1	$1b_1$	12.30	12.34	12.04	12.28	11.95	12.00
1^3B_1	$4a_1$	5.30	5.28	5.31	5.30	5.28	5.29

References

- (1) Dempwolff, A. L.; Paul, A. C.; Belogolova, A. M.; Trofimov, A. B.; Dreuw, A. Intermediate state representation approach to physical properties of molecular electron-detached states. II. Benchmarking. *J. Chem. Phys.* **2020**, *152*, 024125.
- (2) Leitner, J.; Dempwolff, A. L.; Dreuw, A. Fourth-Order Algebraic Diagrammatic Construction for Electron Detachment and Attachment: The IP- and EA-ADC(4) Methods. *J. Phys. Chem. A* **2024**, *128*, 7680–7690.
- (3) Ranasinghe, D. S.; Margraf, J. T.; Perera, A.; Bartlett, R. J. Vertical valence ionization potential benchmarks from equation-of-motion coupled cluster theory and QTP functionals. *J. Chem. Phys.* **2019**, *150*, 074108.
- (4) Dempwolff, A. L.; Belogolova, A. M.; Trofimov, A. B.; Dreuw, A. Intermediate state representation approach to physical properties of molecular electron-attached states: Theory, implementation, and benchmarking. *J. Chem. Phys.* **2021**, *154*, 104117.